Role of three-body dynamics in nucleon-deuteron correlation functions

M. Viviani [1,*] S. König [2,†] A. Kievsky [1,‡] L. E. Marcucci [3,1,§] B. Singh [4,‖] and O. Vázquez Doce [5,¶]

[1]*Istituto Nazionale di Fisica Nucleare, Sezione di Pisa, Largo B. Pontecorvo 3, 56127 Pisa, Italy*
[2]*Department of Physics, North Carolina State University, Raleigh, North Carolina 27695, USA*
[3]*Dipartimento di Fisica, Università di Pisa, Largo B. Pontecorvo 3, 56127 Pisa, Italy*
[4]*Physics Department, TUM, James-Franck-Straße 1, Garching bei München 85748, Germany*
[5]*Istituto Nazionale di Fisica Nucleare, Laboratori Nazionali di Frascati, Via Enrico Fermi 54, Frascati 00044, Italy*

(Received 22 June 2023; accepted 11 October 2023; published 5 December 2023)

Correlation functions of hadrons can be accessed in high-energy collisions of atomic nuclei, revealing information about the underlying interaction. This work complements experimental efforts to study nucleon-deuteron Nd—with $N = p$ (proton) or $N = n$ (neutron)—correlations with theory evaluations using different techniques. The correlation functions C_{nd} and C_{pd} are calculated based on a scattering wave function, extending previous benchmarks for the Nd scattering matrix to this new observable. We use hyperspherical harmonics and Faddeev techniques with one of the widely used nucleon-nucleon (NN) interactions, the Argonne v_{18} potential. Moreover, in the low-energy region we perform additional calculations in the framework of pionless effective field theory. The pd correlation function is computed in the large-energy region to make contact with a recent measurement by the ALICE Collaboration. We show that the scattering wave function has the proper dynamical input to describe an initial rise and subsequent oscillations of C_{pd} as a function of the energy. Effects on the observables using different NN and three-nucleon potentials are evaluated with the conclusion that variations of around 2% are observed. Although these effects are small, future measurements can go beyond this accuracy, allowing for new detailed studies of strong interaction in light nuclear systems. The present study supports the current efforts devoted to the measurement of correlation functions in systems dominated by the strong interactions, such as pd, ppp, Λd, and $pp\Lambda$.

DOI: 10.1103/PhysRevC.108.064002

I. INTRODUCTION

The study and description of the dynamics of few-body systems comprised of nucleons and atomic nuclei play a fundamental role in nuclear physics. A comprehensive understanding of the nuclear force between nucleons inside nuclei and in a denser environment requires an accurate understanding of the few-body dynamics, and achieving this has been a long-standing goal of nuclear physics for many years. In this regard, few- and many-body systems provide a unique laboratory for studying nuclear interactions and the equation of state of dense nuclear matter [1–3]. In recent decades, modern many-body nuclear physics advances have opened doors to study nucleon-nucleus and nucleus-nucleus scattering and reactions from first principles (see Refs. [4–7] and references therein). Nucleon-deuteron (Nd) scattering is a fundamental process in nuclear physics that plays a crucial role in understanding structure and dynamics of atomic nuclei. The deuteron, composed of one proton and one neutron, is the simplest nucleus in nature that is bound together by a strong force. Studying its interaction with another nucleon serves as a test bed for studying three-nucleon effects. This includes not only the occurrence of genuine three-nucleon forces (3NFs)—effects arising not merely from pairwise two-body interactions—but also the interplay of the nuclear interaction with the Pauli principle, i.e., the fact that nucleons as fermions need to have fully antisymmetric wave functions at the quantum level. The three-nucleon system is the simplest system where these effects can be studied, and several methods exist to investigate it theoretically with great precision.

Experimentally, the study of the Nd scattering process has a long history dating back to the early days of nuclear physics, which includes various techniques, such as scattering experiments, polarization measurements, and reactions induced by electroweak probes [8,9]. These measurements have revealed a rich and complex structure that is determined by the interplay between various aspects of the nuclear force, such as one-pion exchange, repulsive and attractive components, and the tensor force. Moreover, in the pd case, the Coulomb force has to be considered as well, and its effect is particularly relevant at low energies [10] and when the two protons emerge with relatively small energy [11].

Theoretically, Nd scattering was initially studied based on potential models. In the 1990s, realistic nuclear potentials

*michele.viviani@pi.infn.it
†skoenig@ncsu.edu
‡alejandro.kievsky@pi.infn.it
§laura.elisa.marcucci@unipi.it
‖bhawani.singh@tum.de
¶oton.vazquezdoce@lnf.infn.it

describing the NN interactions were constructed by fitting the NN world database [12–14], consisting of more than 4000 pp and np data at the time, with a χ^2 per datum close to one. With the development of the effective field theories (EFTs), potential models appeared constructed order by order in a series expansion of the interaction. At present, EFT potentials based on chiral effective field theory (chiral EFT) are available going up to fifth order in the expansion and they reproduce the NN scattering data up to 350 MeV laboratory energy with extremely good accuracy [15,16]. Starting with Ref. [17], focus on the development of chiral EFT has shifted towards applying the expansion directly to observables, investigating in particular questions of renormalization and details of the so-called power counting, i.e., the process of assigning orders to individual components of the interaction. For a review of these efforts and of nuclear effective field theories in general, see Ref. [18].

Beyond the two-nucleon sector that is for the most part used to constrain parameters of the interaction, the three-nucleon system is the simplest scenario in which highly accurate nuclear potentials can be used to make predictions. For this reason strong efforts have been made in the last years to solve the equations that govern the three-nucleon dynamics in bound states and scattering processes. The necessity of including 3NFs was known for a long time, mainly motivated by the fact that highly accurate two-nucleon potentials would typically predict the triton binding energy below its experimentally known value. One of the early successes of nuclear EFTs was the *a priori* prediction that such forces are present and in fact required. The impact of the 3NFs in the three- and four-nucleon continuum is at present under investigation. In particular, although the chiral expansion nicely organizes the importance of different three-nucleon interaction terms, only those terms appearing at the lowest orders have been considered so far. There are indications that subleading three-nucleon interaction terms, though small, improve the description of polarization observables [19].

In the present study, we focus on the Nd correlation function (defined in more detail in the next section). The primary motivation for this work is that precise measurements of correlations in the momentum space for the pd system have been made available by the ALICE Collaboration using proton-proton (pp) collisions at the Large Hadron Collider (LHC). These experiments are performed at very high energy (for example the ALICE Collaboration analyzes data taken at LHC with beam energies in the range of TeV). However, it is possible to detect hadrons (protons, deuterons, or also hyperons, etc.) that are emerging in almost the same direction and with almost the same energy, and then the relative energy between such particles can be very small, ranging from a fraction of a MeV to tens of MeV. In this regime, the mutual interaction between the fragments plays a very important role, reflected in interesting structures in the correlation functions.

For the case of detecting two outgoing protons, the ALICE Collaboration has previously measured the correlation function using the so-called femtoscopy technique [20–22]. The experimental data can be compared with theoretical calculations by evaluating the integral

$$C_{pp}(k) = \int d^3r\, S(\mathbf{r})\, |\psi_k(\mathbf{r})|^2, \tag{1}$$

where $S(\mathbf{r})$ is a source function that parametrizes the distance $\mathbf{r}$ at which the two protons are emitted after the high-energy collision, and ψ_k is the pp scattering wave function depending on the reduced relative momentum of the pair ($k = |\mathbf{p}_2 - \mathbf{p}_1|/2$). An extremely accurate description of this observable was obtained using the Argonne v_{18} (AV18) NN interaction [12]. As we discuss in detail in the following section, the extension of the formalism to handle the Nd case is not trivial because the wave function needs to account for the three-nucleon dynamics mentioned above. We develop in this work a framework that includes all relevant complexities related to the correct description of the system, including antisymmetrization effects. Moreover, the concept of the source function, which for the pp correlation function is related to the emission of two nucleons and can be precisely characterized [22], has to be extended to the case of three emitted nucleons, two of which form a deuteron. Note that pd correlations in momentum space were investigated in the past at lower energies in O-Au and Ar-Ni reactions [23–26]. For these reactions, a precise knowledge of the source sizes was missing. In such heavy systems and at such low energies, the source sizes are expected to be sizably larger, and consequently the sensitivity of the correlation function to the strong interaction smaller.

Since this is the first time that this observable is analyzed for a three-nucleon system, we find it useful to employ two different approaches to solve the three-body dynamics, the solution of the Faddeev equations and the hyperspherical harmonic (HH) technique. Moreover, for the nuclear interaction we consider both the AV18 potential, supplemented by the Urbana IX (UIX) 3NF [27], and, to make contact with the modern EFT description of the nuclear interaction, we additionally use pionless EFT to calculate the correlation function. This EFT has the advantage that its power counting and renormalization properties are well understood. However, since by construction this theory does not explicitly include the physics of pion exchange, its regime of validity is limited to the low-energy region. In addition, we also perform a calculation using a two- and three-nucleon potential model derived within chiral EFT, one of the so-called Norfolk interactions [28], the NVIa + 3N in the notation of Ref. [29]. In the analysis of the correlation function with such highly accurate NN potentials, particular attention will be given to the effects of the accompanying three-nucleon forces.

The paper is organized in the following way: In the next section, we describe the theoretical formalism for the calculation of the Nd correlation functions. In particular, in Sec. II A we discuss the basic formalism for three-nucleon correlations before we move on to review the HH (Sec. II B) and Faddeev (Sec. II C) formalisms, along with a brief introduction to pionless EFT. The main results and benchmarks comparing the different techniques used are given in Sec. III. We conclude with a summary and outlook in Sec. IV.

II. FORMALISM

A. Full three-body calculations of the nucleon-deuteron correlation function

The two-particle femtoscopic correlation function is defined as the ratio of the Lorentz-invariant yield of a particle pair to the product of the single-particle yields. Using $\mathbf{p}_i$ to denote the momentum of each particle, it can be written as [30]

$$C(\mathbf{p}_1,\mathbf{p}_2) = \frac{E_1E_2\,dN^{12}/(d^3p_1\,d^3p_2)}{(E_1\,dN^1/d^3p_1)(E_2\,dN^2/d^3p_2)} = \frac{\mathcal{P}(\mathbf{p}_1,\mathbf{p}_2)}{\mathcal{P}(\mathbf{p}_1)\mathcal{P}(\mathbf{p}_2)}. \tag{2}$$

As indicated by the final equality in Eq. (2), the correlation function can also be understood as the ratio between $\mathcal{P}(\mathbf{p}_1,\mathbf{p}_2)$, the probability of finding a pair of particles with momenta $\mathbf{p}_1$ and $\mathbf{p}_2$, and $\mathcal{P}(\mathbf{p}_i)$, the probability of finding each particle with momentum $\mathbf{p}_i$. In the absence of any correlations, the two-particle probability factorizes, $\mathcal{P}(\mathbf{p}_1,\mathbf{p}_2) = \mathcal{P}(\mathbf{p}_1)\mathcal{P}(\mathbf{p}_2)$, and the correlation function is equal to unity. In the quantum mechanical description, the correlation between a pair of particles (with spins s_1 and s_2, respectively) can be related to the particle emission and the subsequent interaction of the particle pair, as discussed in Ref. [31], as

$$C(\mathbf{p}_1,\mathbf{p}_2) = \frac{1}{\Gamma}\sum_{m_1,m_2}\int d^3r_1\,d^3r_2 S_1(r_1)S_1(r_2) \times|\Psi_{m_1,m_2}(\mathbf{p}_1,\mathbf{p}_2,\mathbf{r}_1,\mathbf{r}_2)|^2, \tag{3}$$

where $\Psi_{m_1,m_2}(\mathbf{p}_1,\mathbf{p}_2,\mathbf{r}_1,\mathbf{r}_2)$ denotes the two-particle scattering wave function that asymptotically describes particle 1 (2) with momentum $\mathbf{p}_1$ ($\mathbf{p}_2$) and spin projection m_1 (m_2), with weights $\Gamma = (2s_1+1)(2s_2+1)$. In Eq. (3), $S_1(r)$ describes the spatial shape of the source for single-particle emissions. It can be approximated as a Gaussian probability distribution with a width R_M, which is defined as follows:

$$S_1(r) = \frac{1}{\left(2\pi R_M^2\right)^{\frac{3}{2}}}e^{-r^2/2R_M^2}. \tag{4}$$

R_M is also known as the source size for single-particle emission. In general, a more realistic source is thought to have an exponential tail caused by resonance-decay contributions [22,32]. In this paper, since we are interested in setting the framework of the calculation of the correlation function for a three-nucleon system, we have not tackled this question and worked with the source given in Eq. (4). Equation (3) can be simplified by noting that in the wave functions the dependence on the overall center-of-mass (c.m.) coordinate can be trivially factored out. Introducing the c.m. coordinate $\mathbf{R} \equiv \frac{M_1\mathbf{r}_1+M_2\mathbf{r}_2}{M_1+M_2}$, where M_1 and M_2 are the masses of the two particles, the relative distance $\mathbf{r} \equiv \mathbf{r}_1 - \mathbf{r}_2$, and rewriting the two-particle wave function as $\Psi_{m_1,m_2}(\mathbf{p}_1,\mathbf{p}_2,\mathbf{r}_1,\mathbf{r}_2) = e^{-i\mathbf{R}\cdot\mathbf{P}}\psi_{m_1,m_2,\mathbf{k}}(\mathbf{r})$ leads to the Koonin-Pratt relation for the two-particle correlation function [33], which we write here as

$$C(k) = \frac{1}{\Gamma}\sum_{m_1,m_2}\int d^3r\,S(r)|\psi_{m_1,m_2,\mathbf{k}}(\mathbf{r})|^2, \tag{5}$$

where $\psi_{m_1,m_2,\mathbf{k}}(\mathbf{r})$ represents the two-particle relative wave function, with $\mathbf{k} = (\mathbf{p}_1 - \mathbf{p}_2)/2$, and $S(r)$ is the two-particle emission source, given by

$$S(r) = \left(\frac{1}{4\pi R_{\rm M}^2}\right)^{3/2} e^{-\frac{r^2}{4R_{\rm M}^2}}. \tag{6}$$

Overall, we have arrived, essentially, at Eq. (1) as stated in the Introduction. We note that for simplicity we did not consider spin degrees of freedom in writing Eq. (1), and moreover the scattering wave function ψ_k used in the Introduction includes all partial waves. A more detailed discussion of how the partial-wave expanded form can be obtained from this will be given for the three-body case below.

For the extension of the formalism to calculate three-nucleon correlation functions, we follow the general coalescence model as it has been discussed in Ref. [31]. For the specific case of nucleon-deuteron correlations, the formalism is based on the following expressions:

$$A_dC_{Nd}(k) = \frac{1}{6}\sum_{m_2,m_1}\int d^3r_1d^3r_2d^3r_3\;S_1(r_1)S_1(r_2)S_1(r_3) \times\left|\Psi^{Nd}_{m_2,m_1,\mathbf{k}}\right|^2, \tag{7a}$$

$$A_d = \frac{1}{3}\sum_{m_2}\int d^3r_1d^3r_2\;S_1(r_1)S_1(r_2)\left|\varphi^d_{m_2}\right|^2, \tag{7b}$$

where $\mathbf{k}$ is the Nd relative momentum and A_d the "probability of formation of the deuteron." The subscript N represents either a proton (p) or a neutron (n), and in the following we consider both cases. Hereafter m_1 (m_2) denotes the spin projection of the nucleon (deuteron). We also denote the deuteron bound-state wave function as $\varphi^d_{m_2}$, whereas $\Psi^{Nd}_{m_2,m_1,\mathbf{k}}$ represents the nucleon-deuteron scattering wave function. In the above equations we indicate explicitly sums over angular momentum components m_1 and m_2, but we note that whether or not these appear explicitly in practical calculations depends on the method used to solve the equations: we consider both an approach based on HH, where m_1 and m_2 are explicitly summed over, as well as Faddeev equations in momentum space, where these sums are implicit in the choice of basis.

Equation (7) can be simplified by introducing the c.m. and relative coordinates, as well. For A_d, we change integration variables, introducing $\mathbf{r} = \mathbf{r}_1 - \mathbf{r}_2$ and $\mathbf{R} = \frac{1}{2}(\mathbf{r}_1 + \mathbf{r}_2)$ (we disregard the proton-neutron mass difference in this paper). Writing the product $S_1(r_1)S_1(r_2)$ in terms of r and R and then integrating over $\mathbf{R}$, one obtains

$$A_d = \frac{1}{3}\sum_{m_2}\int d^3r\;\frac{e^{-r^2/4R_M^2}}{\left(4\pi R_M^2\right)^{\frac{3}{2}}}\left|\varphi^d_{m_2}\right|^2. \tag{8}$$

In integral (7a), we can use the variables

$$\mathbf{x} = \mathbf{r}_1 - \mathbf{r}_2, \quad \mathbf{y} = \mathbf{r}_3 - \frac{\mathbf{r}_1+\mathbf{r}_2}{2}, \quad \mathbf{R}_3 = \frac{1}{3}(\mathbf{r}_1+\mathbf{r}_2+\mathbf{r}_3). \tag{9}$$

Now

$$d^3r_1d^3r_2d^3r_3 = d^3R_3d^3xd^3y, \tag{10}$$

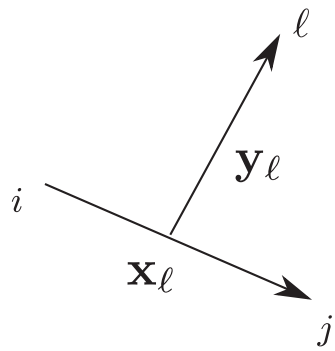

FIG. 1. Definition of the Jacobi vector $\mathbf{x}_\ell$ and $\mathbf{y}_\ell$.

and

$$S_1(r_1)S_1(r_2)S_1(r_3) = \frac{e^{-(3R_3^2+\frac{2}{3}y^2+\frac{1}{2}x^2)/2R_M^2}}{\left(2\pi R_M^2\right)^{\frac{9}{2}}}. \tag{11}$$

Integrating over d^3R_3 (the wave function $\Psi^{Nd}_{m_2,m_1,\mathbf{k}}$ does not depend on R_3), we obtain

$$A_d C_{Nd}(k) = \frac{1}{6}\sum_{m_2,m_1}\int d^3x d^3y \, \frac{e^{-(\frac{4}{3}y^2+x^2)/4R_M^2}}{\left(3\pi R_M^2\right)^{\frac{3}{2}}\left(4\pi R_M^2\right)^{\frac{3}{2}}} \times\left|\Psi^{Nd}_{m_2,m_1,\mathbf{k}}\right|^2. \tag{12}$$

Introducing the vectors $\xi_1 = \sqrt{\frac{4}{3}}\mathbf{y}$ and $\xi_2 = \mathbf{x}$, this integral can be rewritten as

$$A_d C_{Nd}(k) = \frac{1}{6}\sum_{m_2,m_1}\left(\frac{3}{4}\right)^{\frac{3}{2}}\int d^3\xi_1 d^3\xi_2 \times\frac{e^{-(\xi_1^2+\xi_2^2)/4R_M^2}}{\left(3\pi R_M^2\right)^{\frac{3}{2}}\left(4\pi R_M^2\right)^{\frac{3}{2}}}\left|\Psi^{Nd}_{m_2,m_1,\mathbf{k}}\right|^2. \tag{13}$$

Let us now introduce the so-called hyperradius, defined as $\rho = \sqrt{\xi_1^2+\xi_2^2}$, and the hyperangle variables Ω [34] (see below), such that $d^3\xi_1 d^3\xi_2 = \rho^5 d\rho d\Omega$. Finally, we obtain

$$A_d C_{Nd}(k) = \frac{1}{6}\sum_{m_2,m_1}\int \rho^5 d\rho d\Omega \, \frac{e^{-\rho^2/4R_M^2}}{\left(4\pi R_M^2\right)^3}\left|\Psi^{Nd}_{m_2,m_1,\mathbf{k}}\right|^2. \tag{14}$$

As a check of this formula, let us approximate the Nd wave function by the following asymptotic structure, properly antisymmetrized:

$$\Psi^{Nd}_{m_2,m_1,\mathbf{k}} = \frac{1}{\sqrt{3}}\left[e^{i\mathbf{k}\cdot\mathbf{y}_3}\varphi^d_{m_2}(1,2)\chi_{m_1}(3) + e^{i\mathbf{k}\cdot\mathbf{y}_1}\varphi^d_{m_2}(2,3)\chi_{m_1}(1) + e^{i\mathbf{k}\cdot\mathbf{y}_2}\varphi^d_{m_2}(3,1)\chi_{m_1}(2)\right], \tag{15}$$

where $\mathbf{y}_\ell$ are defined below in Eq. (18) (see also Fig. 1, and note that $\mathbf{x}_3 \equiv \mathbf{x}$ and $\mathbf{y}_3 \equiv \mathbf{y}$). We work here with the form given in Eq. (12). For $k \to \infty$, we can disregard the terms coming from different permutations in $|\Psi^{Nd}_{m_2,m_1,\mathbf{k}}|^2$, as $e^{-i\mathbf{k}\cdot\mathbf{y}_3} \times e^{i\mathbf{k}\cdot\mathbf{y}_2}$, as their contribution becomes vanishing. We have three terms left. However, it results in

$$\tfrac{4}{3}y^2 + x^2 = \rho^2 = \tfrac{4}{3}y_\ell^2 + x_\ell^2, \;\; \ell = 1,2,3. \tag{16}$$

Therefore, each of the three terms gives the same contribution canceling the factor $(1/\sqrt{3})^2$, and one obtains

$$\begin{aligned} A_d C_{Nd}(k) &= \frac{1}{6}\sum_{m_2,m_1}\int d^3x d^3y \, \frac{e^{-(\frac{4}{3}y^2+x^2)/4R_M^2}}{\left(3\pi R_M^2\right)^{\frac{3}{2}}\left(4\pi R_M^2\right)^{\frac{3}{2}}} \times\left|\varphi^d_{m_2}(1,2)\right|^2, \\ &= \frac{1}{2}\sum_{m_1}\int d^3y \, \frac{e^{-(\frac{4}{3}y^2)/4R_M^2}}{\left(3\pi R_M^2\right)^{\frac{3}{2}}} A_d, \\ &= A_d. \end{aligned} \tag{17}$$

Therefore, in this case $C_{Nd}(k \to \infty) = 1$ as expected.

B. Hyperspherical harmonics description of the proton-deuteron wave function

We discuss the calculation of the proton-deuteron correlation function by taking into account the full dynamics of the three particles. Initially, we include only the effect of the long-range Coulomb interaction between the proton and the deuteron. However, we still take into account the antisymmetrization of the wave function. This simple scenario will allow us to subsequently address the full case including the short-range nuclear interaction. In the following, for a given permutation $ij\ell$ of the three nucleons, we define the Jacobi coordinates (see Fig. 1)

$$\mathbf{x}_\ell = \mathbf{r}_j - \mathbf{r}_i, \quad \mathbf{y}_\ell = \mathbf{r}_\ell - \frac{\mathbf{r}_i + \mathbf{r}_j}{2}. \tag{18}$$

To construct an antisymmetric wave function it is sufficient to consider the three "even" permutations of the three particles, namely, $ij\ell = 123$, 231, and 312. For this reason, we can specify the permutation (and the various quantities) just giving the value of $\ell = 1, 2, 3$.

We introduce here also the hyperangular coordinates. The hyperradius ρ and hyperangles φ_ℓ are defined in terms of the moduli of the Jacobi vectors, explicitly

$$\rho = \sqrt{x_\ell^2 + \frac{4}{3}y_\ell^2}, \;\; \tan\varphi_\ell = \sqrt{\frac{4}{3}}\frac{y_\ell}{x_\ell}. \tag{19}$$

The hyperradius ρ turns out to be independent on the permutation ℓ. In fact, it can be shown that $\rho^2 = \frac{2}{3}(r_{12}^2 + r_{13}^2 + r_{23}^2)$, where r_{ij} is the distance between particles i and j. The set of hyperangular and angular variables is denoted with Ω_ℓ, namely,

$$\Omega_\ell \equiv \{\varphi_\ell, \hat{\mathbf{x}}_\ell, \hat{\mathbf{y}}_\ell\}, \tag{20}$$

where $\hat{\mathbf{x}}_\ell$ ($\hat{\mathbf{y}}_\ell$) denotes the polar angles of vector $\mathbf{x}_\ell$ ($\mathbf{y}_\ell$). When the permutation index is not indicated the reference order of the particles $ij\ell = 123$ is understood.

1. Free case

Let us consider the free case, i.e., no nuclear interaction between the p and d clusters. The wave function is then simply

given by

$$\Psi^{pd,(\text{free})}_{m_2,m_1,\mathbf{k}} = \frac{1}{\sqrt{3}} \sum_{\ell}^{\text{even perm.}} \varphi^d_{m_2}(i,j)\chi_{m_1}(\ell)\Phi_c(\mathbf{k},\mathbf{y}_\ell), \quad (21)$$

where, as before, $\varphi^d_{m_2}(i,j)$ is the deuteron wave function with spin projection m_2, $\mathbf{k}$ is the relative momentum between the two clusters, $\chi_{m_1}(\ell)$ is a spinor describing the proton, and $\Phi_c(\mathbf{k},\mathbf{y}_\ell)$ is a Coulomb-distorted plane wave, having the following partial-wave expansion:

$$\Phi_c(\mathbf{k},\mathbf{y}) = \sum_{LM} 4\pi\, i^L\, Y^*_{LM}(\hat{\mathbf{k}})Y_{LM}(\hat{\mathbf{y}})e^{i\sigma_L}\frac{F_L(\eta,ky)}{ky}. \quad (22)$$

Here $F_L(\eta,ky)$ is the regular Coulomb function and σ_L the Coulomb phase shift. The neutron-deuteron case can be recovered just replacing $\Phi_c(\mathbf{k},\mathbf{y}_\ell) \to e^{i\mathbf{k}\cdot\mathbf{y}_\ell}$.

Before we address the fully interacting case, it is convenient to expand the free wave function (21) using Eq. (22) and rewrite it as a sum of terms with definite total angular momentum J. Using one of the possible choices of the recoupling order, we obtain

$$\begin{aligned}\Psi^{pd,(\text{free})}_{m_2,m_1,\mathbf{k}} = &\sum_{LSJ}\sqrt{4\pi}i^L\sqrt{2L+1}e^{i\sigma_L}\\ &\times\left(1m_2\frac{1}{2}m_1\middle|SJ_z\right)(L0SJ_z\mid JJ_z)\\ &\times\frac{1}{\sqrt{3}}\sum_{\ell}^{\text{even perm.}}\left\{Y_L(\hat{\mathbf{y}}_\ell)\left[\varphi^d_{m_2}(i,j)\chi_{m_1}(\ell)\right]_S\right\}_{JJ_z}\\ &\times\frac{F_L(\eta,ky_\ell)}{ky_\ell}, \end{aligned} \quad (23)$$

where we have assumed $\hat{\mathbf{k}}//\hat{\mathbf{z}}$ and therefore $Y_{LM}(\hat{\mathbf{k}}) = \frac{\sqrt{2L+1}}{\sqrt{4\pi}}\delta_{M,0}$. Note that $J_z = m_1 + m_2$.

2. Fully interacting case

Now, let us consider the fully interacting case. The total wave function becomes

$$\begin{aligned}\Psi^{pd}_{m_2,m_1,\mathbf{k}} = &\sum_{LSJ}\sqrt{4\pi}i^L\sqrt{2L+1}e^{i\sigma_L}\left(1m_2\frac{1}{2}m_1\middle|SJ_z\right)\\ &\times(L0SJ_z\mid JJ_z)\Psi_{LSJJ_z}, \end{aligned} \quad (24)$$

where Ψ_{LSJJ_z} are three-body wave functions satisfying $(H-E)\Psi_{LSJJ_z} = 0$, with

$$E = \frac{4}{3}\frac{k^2}{M_N} - B_d, \quad (25)$$

where B_d denotes the deuteron binding energy and M_N is the nucleon mass. We compute such wave functions as

$$\begin{aligned}\Psi_{LSJJ_z} = &\sum_{n,\alpha}\frac{u_{n,\alpha}(\rho)}{\rho^{5/2}}\mathcal{Y}_{n,\alpha}(\Omega)\\ &+\frac{1}{\sqrt{3}}\sum_{\ell}^{\text{even perm.}}\{Y_L(\hat{\mathbf{y}}_\ell)[\varphi^d(i,j)\chi(\ell)]_S\}_{JJ_z}\\ &\times\frac{F_L(\eta,ky_\ell)}{ky_\ell} + \sum_{L'S'}T^J_{LS,L'S'}\frac{1}{\sqrt{3}}\\ &\times\sum_{\ell}^{\text{even perm.}}\{Y_{L'}(\hat{\mathbf{y}}_\ell)[\varphi^d(i,j)\chi(\ell)]_{S'}\}_{JJ_z}\\ &\times\frac{\overline{G}_{L'}(\eta,ky_\ell)+iF_{L'}(\eta,ky_\ell)}{ky_\ell}. \end{aligned} \quad (26)$$

Here $\mathcal{Y}_{n,\alpha}(\Omega)$ is a set of completely antisymmetric basis functions constructed in terms of HH functions (which form a complete basis in the Ω Hilbert space) multiplied by appropriate combinations of spin-isospin states of the three particles. Explicitly,

$$\begin{aligned}\mathcal{Y}_{n,\alpha}(\Omega) = &\sum_{\ell}^{\text{even perm.}} f_\alpha(x_\ell)\mathcal{N}_\alpha(\sin\phi_\ell)^{L_y}(\cos\phi_\ell)^{L_x}\\ &\times P_n^{L_y+\frac{1}{2},L_x+\frac{1}{2}}(\cos 2\phi_\ell)\\ &\times\{[Y_{L_y}(\hat{\mathbf{y}}_\ell)Y_{L_x}(\hat{\mathbf{x}}_\ell)]_\Lambda[(s_is_j)_{S_2}s_\ell]_\Sigma\}_{JJ_z}\\ &\times[(t_it_j)_{T_2}t_\ell]_{T,T_z}, \end{aligned} \quad (27)$$

where $\alpha \equiv \{L_x, L_y, \Lambda, S_2, \Sigma, T_2, T\}$ is a set of quantum numbers specifying the HH functions, $P_n^{a,b}$ a Jacobi polynomial of degree n, and $\mathcal{N}$ suitable normalization factors. Moreover, to accelerate the convergence of the expansion over n, we have added the so-called correlation factors $f_\alpha(x_\ell)$, chosen in order to reproduce the behavior of the wave function when the particles i and j are close (and thus the distance x_ℓ is small). These functions describe the two-body correlations of the wave functions, and clearly they depend on the spin-isospin-angular state of the pair (i.e., by the quantum numbers α). The expansion so organized is called pair-correlated HH (PHH) expansion. For a discussion of the choice of the functions f_α and a review of the properties of the HH and PHH states, see, for example, Refs. [34,35].

The calculation is performed as follows. For a given choice of the quantum number α (called a "channel"), the functions given in Eq. (27) with increasing values of n are considered, up to a value N_α, chosen so to have a convergence of the quantities of interest, as the phase shifts. Thanks to the presence of the correlation factor, a very good convergence is obtained already with low values of N_α; typically $N_\alpha = 5$–10 is sufficient. Then other channels are included in the expansion, etc. Note that the most important channels are those with low values of L_x and L_y, so we usually start by including in the expansion channels with $L_x + L_y = \mathcal{L} = 0$ or 1, and then increase the value of $\mathcal{L}$. Usually it is sufficient to consider channels up to $\mathcal{L} = 5$ or 6, of a total number ranging from 18 to 30, depending on the value of the total angular momentum and parity J^π. At the end, the expansion over n and α includes some hundreds of terms.

The expansion in the first row of Eq. (26) describes the system when the three nucleons are close to each other. The hyperradial functions $u_{n,\alpha}(\rho)$ are obtained by solving a set of coupled differential equations, obtained using the Kohn variational principle [36,37]. They go asymptotically to zero for energies below the deuteron breakup threshold, whereas

for energies $E \equiv Q^2/m > 0$ [see Eq. (25)], the hyperradial functions $u_{n,\alpha}(\rho) \to A_\alpha e^{iQ\rho}$ when $\rho \to \infty$.

Moreover, in Eq. (26) $T^J_{LS,L'S'}$ are the T-matrix elements, also obtained from the Kohn variational principle, which describe *pd* scattering observables. Above we introduced

$$\overline{G}_{L'}(\eta, ky) = G_{L'}(\eta, ky)(1 - e^{-\beta y})^{(2L'+1)}, \tag{28}$$

$G_{L'}$ being the irregular Coulomb function. With this definition, the regularized irregular Coulomb functions $\overline{G}_{L'}(\eta, ky)$ are well behaved for all values of y, and for $y \gg \beta^{-1}$ they reduce to the irregular Coulomb functions. Typically $\beta = 0.25$ fm^{-1} is used as a regularization scale. In Eq. (26), $L'S'$ are all possible combinations for the given J and parity $(-1)^L$.

The asymptotic behavior of the wave functions Ψ_{LSJJ_z} is chosen so that if we turn off the nuclear interaction they reduce to

$$\Psi_{LSJJ_z} \to \frac{1}{\sqrt{3}} \sum_{\ell}^{\text{even perm.}} \{Y_L(\hat{\mathbf{y}}_\ell)[\varphi^d(i,j)\chi(\ell)]_S\}_{JJ_z} \frac{F_L(\eta, ky_\ell)}{ky_\ell}. \tag{29}$$

In fact, in such a case, $u_\alpha = T^J_{LS,L'S'} = 0$ and $\Psi^{pd}_{m_2,m_1,\mathbf{k}}$ reduces to $\Psi^{pd,(\text{free})}_{m_2,m_1,\mathbf{k}}$. Moreover, the asymptotic behavior is such that the part multiplying the T matrix has a form of an outgoing wave, since $G_{L'}(\eta, ky_\ell) + iF_{L'}(\eta, ky_\ell) \sim e^{iky_\ell}$.

In the calculation, we will include the effect of the nuclear interaction up to a given $\overline{J}$. In fact, for $J > \overline{J}$, the centrifugal barrier should forbid the three particles to be close; in that case the free wave function given by Eq. (29) should be appropriate. Accordingly, it is convenient to resum all the terms proportional to $F_L(\eta, ky_\ell)$ in order to reproduce the free wave function. Let us define

$$\begin{aligned}\widetilde{\Psi}_{LSJJ_z} = &\sum_\alpha \frac{u_\alpha(\rho)}{\rho^{5/2}} \mathcal{Y}_\alpha(\Omega) + \sum_{L'S'} T^J_{LS,L'S'} \\ &\times \frac{1}{\sqrt{3}} \sum_{\ell}^{\text{even perm.}} \{Y_{L'}(\hat{\mathbf{y}}_\ell)[\varphi^d(i,j)\chi(\ell)]_{S'}\}_{JJ_z} \\ &\times \frac{\overline{G}_{L'}(\eta, ky_\ell) + iF_{L'}(\eta, ky_\ell)}{ky_\ell},\end{aligned} \tag{30}$$

where we have subtracted from the wave function given in Eq. (26) the "free" part. Then the total wave function $\Psi^{Nd}_{m_2,m_1,\mathbf{k}}$ can be cast in the form

$$\begin{aligned}\Psi^{pd}_{m_2,m_1,\mathbf{k}} = &\Psi^{pd,(\text{free})}_{m_2,m_1,\mathbf{k}} \\ &+ \sum_{LSJ}^{J\leqslant\overline{J}} \sqrt{4\pi} i^L \sqrt{2L+1} e^{i\sigma_L} \left(1 m_2 \frac{1}{2} m_1 \middle| S J_z\right) \\ &\times (L0SJ_z \mid JJ_z) \widetilde{\Psi}_{LSJJ_z}.\end{aligned} \tag{31}$$

This is the three-nucleon wave function which asymptotically behaves as a *pd* (distorted) plane wave, with the proton (deuteron) in the spin state m_1 (m_2). The components $\widetilde{\Psi}_{LSJJ_z}$ describe configurations where the three particles are close to each other. Varying the value of $\overline{J}$ it is possible to control the waves where the strong interaction is taken into account.

Great care must be taken in order to include a sufficient number of PHH states $\mathcal{Y}_{n,\alpha}(\Omega)$; in particular it is necessary to include a sufficient number of channels α in Eq. (30). This part is essential to describe the configurations where the three particles are close to each other. Partial waves where the convergence of this expansion is more critical are those in which the orbital angular momentum L takes its lowest values, $J^\pi = 1/2^+$, $3/2^+$, $1/2^-$, $3/2^-$, and $5/2^-$. For the $J^\pi = 1/2^+$ case, there is the formation of the ^{3}He bound state and therefore the scattering wave function must be constructed orthogonal to it. For the states with relative orbital angular momentum $L = 1$, the interaction between the three particles is rather attractive; therefore, a large number of terms in the sum over α in Eq. (30) is required.

C. Pionless EFT with momentum-space integral equations

Pionless EFT is designed to capture the universal low-energy features of few-nucleon systems that arise from the fact that the nucleon-nucleon S-wave scattering lengths are large compared to the typical range of the nuclear interaction, set by the inverse pion mass $M_\pi^{-1} \sim 1.4$ fm. The theory is constructed to yield the most general parametrization of the nuclear force within its regime of validity (characterized by the EFT breakdown scale $\sim M_\pi$), and it has been used to make a number of highly precise predictions for low-energy processes (for a recent review of the theory and applications, see Ref. [18]).

The strong nuclear interaction in pionless EFT is described by a series of contact (zero-range) interactions, including an increasing number of derivatives as one goes to subsequently higher order in the EFT expansion. In the two-nucleon sector, this series reproduces the well-known effective range expansion [38], which pionless EFT consistently extends to few- and many-nucleon systems. Pionless EFT in particular captures the universal physics reflecting the closeness of low-energy nuclear systems to the unitarity limit (infinite two-nucleon S-wave scattering lengths). A remarkable feature stemming from this is the appearance of a three-nucleon contact interaction at leading order in the theory [39,40], which one would naively expect to be subleading.

To evaluate the correlation function as defined in Sec. II A in momentum space, in the following section we consider first the general Faddeev formalism for scattering calculations, which is not limited to interactions derived from pionless EFT. Since for the moment we neglect electromagnetic effects, the resulting expressions will be valid for calculations of neutron-deuteron correlation functions. For the proton-deuteron system, discussed subsequently in Sec. II C 2, we will instead use equations derived directly from a diagrammatic approach, which we relate to general formalism.

1. *Faddeev approach for neutron-deuteron scattering*

We will follow here largely Ref. [41], with some differences, and begin with an overview of the homogeneous Faddeev equation that describes bound states. Neglecting three-nucleon forces, the basic Faddeev equation for the three-

nucleon bound-state problem can be written as

$$|\psi\rangle = G_0 t P\,|\psi\rangle\,, \tag{32}$$

where $|\psi\rangle$ denotes one of three equivalent Faddeev components, G_0 is the free three-nucleon Green's function, t denotes the two-nucleon T matrix, and P is a permutation operator defined as

$$P = P_{12}P_{23} + P_{13}P_{23}. \tag{33}$$

For definiteness, we use here the convention that $|\psi\rangle$ are the Faddeev components with nucleons 1 and 2 singled out. Therefore, t acts within the (12) subsystem, and in order to represent the equations in momentum space we use Jacobi momenta $\mathbf{u}_1 = \frac{1}{2}(\mathbf{k}_1 - \mathbf{k}_2)$ and $\mathbf{u}_2 = \frac{2}{3}[\mathbf{k}_3 - \frac{1}{2}(\mathbf{k}_1 + \mathbf{k}_2)]$, where $\mathbf{k}_i$ are the individual nucleon momenta. Note that $\mathbf{u}_1$ and $\mathbf{u}_2$ are the momenta conjugate to the Jacobi coordinates $\mathbf{x}$ and $\mathbf{y}$, respectively, that were introduced previously. Projecting the three-dimensional momenta onto partial waves yields states $|u_1 u_2; s\rangle$, where

$$|s\rangle = \left|\left(l_2\left((l_1 s_1) j_1 \tfrac{1}{2}\right) s_2\right) J; \left(t_1 \tfrac{1}{2}\right) T\right\rangle \tag{34}$$

collects angular momentum, spin, and isospin quantum numbers. They are coupled such that $(l_1 s_1) j_1$ and t_1 describe the two-nucleon subsystem, whereas l_2 denotes the orbital angular momentum associated with the Jacobi momentum u_2, and s_2 is an intermediate quantum number. Given a solution $|\psi\rangle$ of Eq. (32), the full three-nucleon wave function can be obtained as

$$|\Psi\rangle = (1 + P)\,|\psi\rangle\,. \tag{35}$$

In order to calculate three-nucleon scattering, we need to consider an inhomogeneous Faddeev equation. Specifically, we are interested here in neutron-deuteron (nd) scattering, and to set up that system we define a state

$$|\phi\rangle = |\varphi_d k; s_d\rangle \tag{36}$$

that is a product of a deuteron state $|\varphi_d\rangle$ in the (12) subsystem and a plane wave $|k\rangle$ that describes the relative motion of the third nucleon with respect to the deuteron. The s_d in Eq. (36) is used to denote a set of three-nucleon quantum numbers restricted to channels that support the existence of a deuteron component, i.e., $|s_d\rangle$ necessarily has $s_1 = 1$, $t_1 = 0$, $j_1 = 1$, and $l_1 = 0$ or 2. In the momentum-space partial-wave representation, we have

$$\langle u_1 u_2; s|\phi\rangle \sim \varphi_d^{(l_1)}(u_1)\frac{\delta(u_2 - k)}{u_2^2}\delta_{s,s_d}, \tag{37}$$

where $\varphi_d^{(l_1)}(u_1)$ is the momentum-space wave function of the deuteron component with angular momentum l_1. In configuration space, if $\mathbf{y}$ denotes the Jacobi coordinate conjugate to $\mathbf{u}_2$, the representation of $|\phi\rangle$ involves a spherical Bessel function $j_{l_2}(ky)$.[1]

[1]For pd scattering, the Bessel function would be replaced by a regular Coulomb wave function.

With the help of $|\phi\rangle$ we can now introduce an operator $\tilde{T}$ that satisfies

$$|\psi_k; s_d\rangle = |\phi\rangle + \tilde{T}\,|\phi\rangle\,, \tag{38}$$

where $|\psi_k\rangle$ is one Faddeev component of the neutron-deuteron scattering state with relative momentum k. Note that this definition is analogous to the definition of the two-body T matrix as the operator that maps a plane-wave state to the full scattering state with the same momentum. The $\tilde{T}$ we use here is related to the operator called T in Ref. [41] by $\tilde{T} = G_0 T$. The inhomogeneous Faddeev equation used to calculate $\tilde{T}$ has the form

$$\tilde{T}\,|\phi\rangle = G_0 t P\,|\phi\rangle + G_0 t P \tilde{T}\,|\phi\rangle\,. \tag{39}$$

For clarity we choose here, unlike most references on the subject, to explicitly write the dependence on $|\phi\rangle$, so really the object that we obtain by solving Eq. (39) is $\tilde{T}\,|\phi\rangle$. Note that working with $\tilde{T}$ instead of T is convenient for our goal of calculating scattering wave functions, but it is by no means a necessary choice: T and $\tilde{T}$ contain exactly the same physics information and one can easily be obtained from the other. For a numerical solution we project Eq. (39) onto the momentum-space partial-wave states $|u_1 u_2; s\rangle$ introduced before. To that end, note that only the total spin J and isospin T (and their projections M_J and M_T that we do not specify explicitly) are conserved quantum numbers for the three-nucleon system. Therefore, in practice we need to fix J and T and include *all* channels $|s\rangle$ for which the intermediate quantum numbers defined in Eq. (34) can couple to the chosen total J and T. From Eq. (39) one therefore obtains a set of *coupled* integral equations, which turn into a set of coupled matrix equations upon discretization of the Jacobi momenta $u_{1,2}$ on a quadrature mesh. We omit here the details of that numerical procedure and instead focus on how to obtain scattering parameters and wave functions from a solution of the equation system obtained via Eq. (39).

In order to obtain elastic scattering parameters, one calculates from $\tilde{T}$ another quantity

$$U\,|\phi\rangle = P G_0^{-1}\,|\phi\rangle + P G_0^{-1}\tilde{T}\,|\phi\rangle\,, \tag{40}$$

and then this needs to be contracted with $\langle\phi'| = \langle\varphi_d k; s'_d|$ from the left to obtain matrix elements $\langle\phi'|U|\phi\rangle$. The dimension of the final matrix is determined by the allowed combinations of quantum numbers l_2 and s_2 for a given fixed total J, whereas l_1 is summed over for each individual matrix element. If standing-wave boundary conditions are chosen for the solution of Eq. (39), the resulting matrix is a K matrix from which it is straightforward to obtain phase shifts and mixing angles after picking a particular representation.

The procedure for calculating scattering wave functions is slightly different. First, Eq. (39) is most conveniently solved with outgoing boundary conditions in order to have direct access to the imaginary part of the amplitude. Instead of U we are now interested directly in the Faddeev component $|\psi_k; s_d\rangle$ as defined in Eq. (38). In order to obtain from this a relative nd wave function in momentum space, we need to project onto an outgoing asymptotic state similarly to what we did to obtain $\langle\phi'|U|\phi\rangle$, except that now we are using $\langle\phi'| = \langle\varphi_d u_2; s'_d|$, with

an arbitrary momentum u_2 and $\langle s'_d|$ such that $l'_2 = l_2$ and $s'_2 = s_2$. Assuming that $|\varphi_d\rangle$ is properly normalized to unity, this yields an expression of the form

$$\langle \varphi_d u_2; s'_d | \psi_k; s_{nd} \rangle = \frac{\delta(u_2 - k)}{k^2} + \langle \varphi_d u_2; s'_d | \tilde{T} | \varphi_d k; s_d \rangle \,. \tag{41}$$

At this point we note that the discussion so far is based only on the single Faddeev component $|\psi_k; s_d\rangle$ and the corresponding amplitude $\tilde{T}$. That is sufficient if one is interested merely in extracting elastic scattering information (via U), and a Fourier-Bessel transformation of Eq. (41) will produce a wave function the (reduced) radial part of which has the appropriate form $\sim \sin(ky + \delta(k))$, which is used, for example, in configuration-space formulations of the Faddeev equations [42]. To actually calculate the *full* scattering wave function, however, we need to use the analog of Eq. (35) for scattering calculations, i.e.,

$$|\Psi_k; s_d\rangle = (1 + P)\, |\psi_k; s_d\rangle \,. \tag{42}$$

Based on this we can then proceed as before and project onto $\langle \phi' | = \langle \varphi_d u_2; s'_d |$. The result involves the same distribution part $\delta(u_2 - k)/k^2$ (which can be seen directly), and its Fourier-Bessel transform will exhibit the same asymptotic behavior $\sim \sin(ky + \delta(k))$, but the antisymmetrization changes the detailed structure at short distances.

In order to evaluate the correlation function within this formulation (without Fourier transformation of the wave functions to coordinate space), we note that the source function $S(r)$ can be written as an operator $\hat{S}$ that is local in coordinate space:

$$\langle \mathbf{r} |\, \hat{S}\, | \mathbf{r}' \rangle = \frac{\exp(-r^2/R^2)}{(4\pi R)^{3/2}} \delta^{(3)}(\mathbf{r} - \mathbf{r}'). \tag{43}$$

In momentum space, this translates to a nonlocal representation that can be written in closed form [43]:

$$\langle q, \ell |\, \hat{S}\, | q', \ell' \rangle = \exp(-R^2(q^2 + q'^2))\, i_\ell(2Rqq')\delta_{\ell\ell'}. \tag{44}$$

In this expression, ℓ denotes the orbital angular momentum of a particular partial wave, and i_ℓ is a modified spherical Bessel function. The scale R is related to the source radius of Sec. II A via $R = \sqrt{3/4} R_M$. Overall, we can now write Eqs. (7a) and (7b) as

$$A_d\, C_{nd}(k) = \sum_{s_d} \alpha(s_d)\, \langle \Psi_k; s_d |\, \hat{S}\, | \Psi_k; s_d \rangle \,, \tag{45a}$$

$$A_d = \langle \varphi_d |\, \hat{S}\, | \varphi_d \rangle \,. \tag{45b}$$

In Eq. (45a) we include a factor

$$\alpha(s_d) = \frac{1}{3} \frac{2J+1}{2 \times 3}, \tag{46}$$

where the $1/3$ in the front is due to the antisymmetrization in Eq. (42), and the rest covers the spin weights for each individual contribution to the correlation function. The factors 2 and 3 in the denominator account for the spin $1/2$ of the neutron and the spin 1 of the deuteron, respectively.

2. *Diagrammatic approach for proton-deuteron scattering*

Coulomb effects in pionless EFT were first studied in Ref. [44] for two nucleons, and in Ref. [45] for proton-deuteron scattering in the $J = 3/2$ channel; Ref. [46] was the first to extend this work to scattering in the $J = 1/2$ channel. Importantly, Ref. [47] established that with a nonperturbative inclusion of Coulomb effects, which is mandatory in the very-low-energy regime, an isospin-breaking correction to leading-order (LO) three-nucleon force enters at next-to-leading order (NLO) in the EFT power counting. At intermediate energies as well as for the trinucleon bound states (^{3}H and ^{3}He), however, Coulomb effects are a perturbative correction [48–50]. In this work we use the nonperturbative treatment in order to describe *pd* scattering from zero energy all the way up to the breakdown scale of the theory, $M_\pi \approx 140$ MeV, in a single unified formulation.

The part of the pionless EFT Lagrangian that is relevant for the present work can be written as

$$\begin{aligned}\mathcal{L} = {} & N^\dagger \left(iD_0 + \frac{\mathbf{D}^2}{2M_N} \right) N - d^{i\dagger} \left[\sigma_d + \left(iD_0 + \frac{\mathbf{D}^2}{4M_N} \right) \right] d^i \\ & - t^{A\dagger} \left[\sigma_t + \left(iD_0 + \frac{\mathbf{D}^2}{4M_N} \right) \right] t^A \\ & + y_d \left[d^{i\dagger} \left(N^T P_d^i N \right) + \text{H.c.} \right] + y_t \left[t^{A\dagger} \left(N^T P_t^A N \right) + \text{H.c.} \right] \\ & + \mathcal{L}_3 + \mathcal{L}_{\text{photon}},\end{aligned} \tag{47}$$

with the nucleon field N (with mass M_N), a doublet in spin and isospin space, and two dibaryon fields d^i (with spin 1 and isospin 0) and t^A (with spin 0 and isospin 1), corresponding to the deuteron and the spin-singlet isospin-triplet virtual bound state in S-wave nucleon-nucleon scattering. Projectors P_d^i and P_t^A are used to select the appropriate quantum numbers for nucleon field bilinears. The formulation in terms of dibaryon fields that we use here is particularly convenient to discuss nucleon-deuteron scattering. It is equivalent to pionless EFT constructed with only nucleon fields in the strong sector, and the coupling constants $y_{d/t}$ and $\sigma_{d/t}$ can be related to the standard low-energy constants $C_{0,d/t}$, $C_{2,d/t}$ that multiply two-nucleon contact interactions. An important feature that arises from the closeness of the low-energy few-nucleon regime to the so-called unitarity (infinite S-wave scattering lengths) limit—close enough, in fact, to permit a perturbative expansion around it [51]—is the presence of a three-nucleon interaction already at LO in the theory, first derived in Refs. [40,52]. We write this interaction in Eq. (47) simply as $\mathcal{L}_3$ and refer to Ref. [18] and the original references above for details.

The coupling of nucleons (and dibaryons) to the electromagnetic (e.m.) field is implemented by the covariant derivative $D_\mu = \partial_\mu + ieA_\mu \hat{Q}$ with the charge operator $\hat{Q}$, $e^2 = 4\pi\alpha$ the e.m. coupling strength, and the photon field A_μ. The photon kinetic term is included in $\mathcal{L}_{\text{photon}}$. In the nonrelativistic low-energy regime considered here, we need only keep the contribution of so-called Coulomb photons, corresponding to a static potential $\sim 4\pi\alpha/(\mathbf{q}^2 + \lambda^2)$ between nucleons, where $\mathbf{q}$ denotes the momentum transfer and λ is a small photon mass (infrared regulator) necessary for a momentum-space

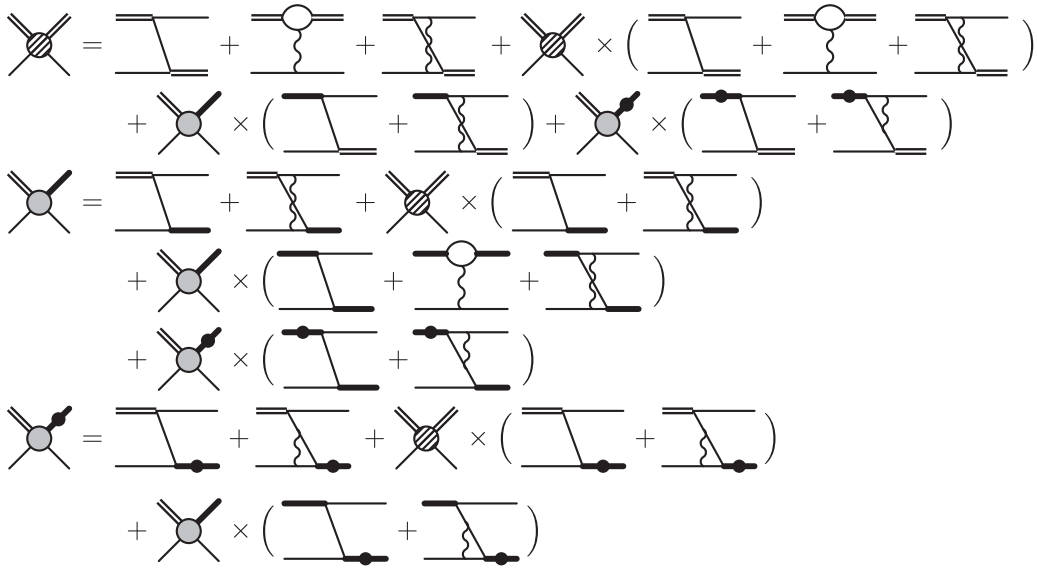

FIG. 2. Coupled-channel integral equation for the full (i.e., strong + Coulomb) proton-deuteron scattering amplitude in the spin-doublet ($S = 1/2$) channels. The diagrams representing the three-nucleon force have been omitted. Notation as in Ref. [46].

formulation of the theory. More details on the formalism can be found in previous publications on the subject (see, e.g., Ref. [46]).

Proton-deuteron scattering in the spin-doublet channels ($S = 1/2$) is described by an integral equation that is shown diagrammatically in Fig. 2. This equation describes an amplitude $\mathcal{T}$, represented by the blob with hatched shading, and involves two coupled channels because in intermediate configurations both spin-triplet and spin-singlet two-nucleon states can appear. These are drawn as double lines and thick lines, respectively. In spin-quartet channels ($S = 3/2$), the Pauli principle prohibits intermediate spin-singlet states, and consequently in this channel the scattering amplitude is given by merely the first row in Fig. 2. For either channel, we numerically implement the integral equation by projecting on a particular spin channel (described by quantum numbers s_d as introduced in the previous section), and by discretizing all momentum integrals (arising from loops in the diagrams) to obtain matrix-vector equations. The full details of this procedure can be found, for example, in Refs. [47,53].

We can relate $\mathcal{T}$ to the scattering amplitude $\tilde{T}$ introduced in Sec. II C 1. If we consider the special case of a separable two-body interaction between nucleons, $V(u, u') = C_0 g(u) g(u')$ for momenta u and u' [where $g(u)$ in an EFT context implements an ultraviolet cutoff for a given regularization scheme], then we can write (neglecting discrete quantum numbers for simplicity)

$$\tilde{T}(u_1, u_2) = g(u_1)\tau\left(M_N E - \tfrac{3}{4}u_2^2\right)G_0(E; u_1, u_2)\tilde{\mathcal{T}}(u_2), \quad (48)$$

where τ expresses the energy dependence of the separable two-nucleon T matrix,

$$t(E; u, u') = g(u)\tau(M_N E)g(u'). \quad (49)$$

For each two-nucleon channel, the T matrix can be obtained by algebraically solving the Lippmann-Schwinger equation for the separable potential V [54], or equivalently by solving an equation that follows from a diagrammatic representation of the "dibaryon propagators" that appear as intermediate states (double and thick lines) in Fig. 2 [47,53].

The relationship between $\tilde{\mathcal{T}}$ and $\mathcal{T}$ is then just a factor,

$$\tilde{\mathcal{T}} = -\frac{M_N}{4\pi}\mathcal{T}, \quad (50)$$

up to potentially different regularization schemes. Specifically, the diagrammatic approach does in fact not use the separable Gaussian regular, but instead imposes a sharp cutoff Λ imposed directly on momentum integrals. This can be interpreted as setting $g(u) = \Theta(\Lambda - u)$, where Θ denotes the unit step function. Note that the details of the running coupling $C_0(\Lambda)$ change with the regulator, but the physics does not depend on this arbitrary choice. Finally, Eqs. (50) and (48) can be combined and inserted into Eq. (41), which then leads to an expression for the pd correlation function $C_{pd}(k)$ via Eqs. (45). To carry out antisymmetrization for the spin-doublet channels, we first combine the two parts shown in the second and third rows of Fig. 2 into a single amplitude in order to then apply an isospin-symmetric recoupling formalism to implement Eq. (35). To conclude this part we note that when the momentum k and therefore the associated energy E is large enough to break up the deuteron ($k \gtrsim 50$ MeV), the Green's function G_0 in Eq. (48) exhibits an on-shell singularity. We account for this effect by adding a small imaginary part $i\eta$ with $\eta \ll E$ to the energy.

3. *Next-to-leading-order calculation*

In a rigorously perturbative setup, as we employ it here, the pd correlation function has an expansion of the form

$$C_{pd}(k) = C_{pd}^{(0)}(k) + C_{pd}^{(1)}(k) + \cdots, \quad (51)$$

where $C_{pd}^{(0)}(k)$ is the LO result, $C_{pd}^{(1)}(k)$ is the NLO correction, and the ellipses represent higher-order corrections that we do not consider in this work. We emphasize that the LO calculation is still performed in a nonperturbative manner at the three-nucleon level, which is necessary at least in the $J^\pi = 1/2^+$ partial wave to generate the ^{3}He bound state, and for convenience applied to all partial waves at leading order. Moreover, the formalism naturally includes the LO two-nucleon interaction nonperturbatively, as mandated by the shallow S-matrix poles associated with the large NN scattering lengths. All corrections applied on top of LO, however, are included via strict distorted-wave perturbation theory, and that is what we refer to as the "rigorously perturbative setup" in this context.

Assuming that the source operator does not have an expansion by itself, the series in Eq. (51) is generated by the EFT expansion of the scattering wave function,

$$|\Psi_k\rangle = \left|\Psi_k^{(0)}\right\rangle + \left|\Psi_k^{(1)}\right\rangle + \cdots , \tag{52}$$

which is, in turn, generated by the expansions for $\tilde{\mathcal{T}}$ and τ [see Eq. (50)]. Moreover, the deuteron wave function has an analogous expansion

$$|\varphi_d\rangle = \left|\varphi_d^{(0)}\right\rangle + \left|\varphi_d^{(1)}\right\rangle + \cdots , \tag{53}$$

which gives rise to an expansion for A_d. Overall, we have

$$A_d^{(0)} C_{pd}^{(0)}(k) = \left\langle \Psi_k^{(0)} \right| \hat{S} \left| \Psi_k^{(0)} \right\rangle \tag{54}$$

at leading order, whereas at NLO we need to extract $C_{pd}^{(1)}(k)$ from

$$A_d^{(0)} C_{pd}^{(1)}(k) + A_d^{(1)} C_{pd}^{(1)}(k) = 2\mathrm{Re}\left\langle \Psi_k^{(0)} \right| \hat{S} \left| \Psi_k^{(1)} \right\rangle . \tag{55}$$

This can be achieved by noting that independently we have $A_d^{(1)} = 2\mathrm{Re}\,\langle\varphi_d^{(0)}|\,\hat{S}\,|\varphi_d^{(1)}\rangle$, and from the LO calculation we already know $C_{pd}^{(0)}(k)$. Hence, we can solve Eq. (55) for $C_{pd}^{(1)}(k)$.

III. RESULTS AND COMPARISON

A. Proton-proton correlation function

Before we consider the nucleon-deuteron correlation function, it is instructive to compare the performance of different nuclear interactions for the pp case. In Fig. 3, we show the pp correlation function $C_{pp}(k)$ calculated with three different approaches. The circles and triangles represent the calculation based on the same AV18 potential that we use for the Nd calculation. For the circles, the nuclear interaction is included only in the S-wave ($^1S_0$) channel, while for the triangles we include the interaction in addition in P- and D-wave channels. In both cases, additional pure Coulomb contributions are included up to a maximum angular momentum $\ell_{\max} = 20$. We observe that the correlation function is completely dominated by the S-wave interaction, with only very small contributions from higher partial waves for momenta above about 70 MeV.

The green band in Fig. 3 shows the result of a pionless EFT calculation at leading order. For this two-body system, the simplest way to implement pionless EFT is by employing

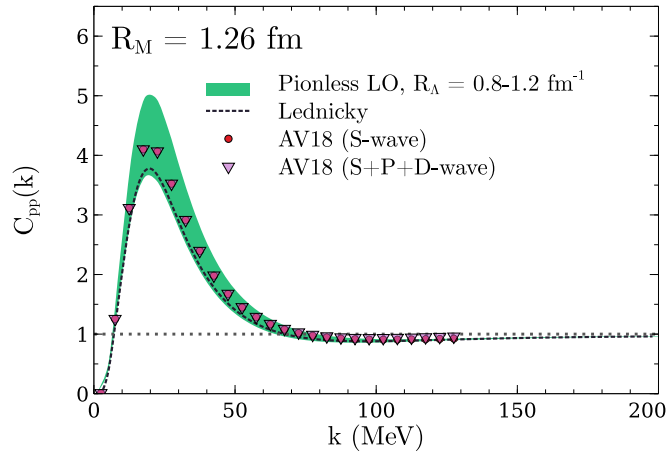

FIG. 3. The proton-proton correlation function $C_{pp}(k)$ as a function of the relative momentum k calculated with different approaches. The symbols show $C_{pp}(k)$ calculated with the AV18 interaction, with circles representing a calculation that includes the nuclear interaction only in the S-wave ($^1S_0$) channel, while for the triangles the interaction is considered also in the P- and D-wave channels (the two results are practically coincident). The shaded band reflects a pionless EFT calculation at leading order for a range of regulator scales (see text for details). The dashed line shows for comparison a calculation based on the Lednický model, as explained in the main text.

a local coordinate-space potential

$$V_{\mathrm{LO},pp}(r) = C_0(R_\Lambda) \exp\left(-\frac{r^2}{R_\Lambda^2}\right) + \frac{\alpha}{r}, \tag{56}$$

where R_Λ is the scale for a local Gaussian regulator (which is roughly related to a momentum cutoff $\Lambda \sim 2/R_\Lambda$). For each choice of R_Λ, renormalization is achieved by adjusting the coefficient $C_0(R_\Lambda)$ such that $V_{\mathrm{LO},pp}(r)$ overall reproduces the experimental value for the pp scattering length, $a_{pp} = -7.806$ fm. The band in the figure is generated by varying R_Λ in the range between 0.8 and 1.2 fm. We note that for this leading-order calculation only the scattering length is reproduced exactly, while the next term in the (Coulomb-modified) effective range expansion, namely, the pp effective range, is only induced by the regulator. The center of the band shown in Fig. 3 roughly corresponds to $R_\Lambda = 1.0$ fm, whereas we find the induced effective range closest to the actual experimental value near $R_\Lambda = 1.1$ fm. This observation gives good reason to expect that a proper next-to-leading-order calculation—which would fix a second parameter to reproduce the effective exactly for any R_Λ—will narrow the band close to the AV18 result.

Finally, the dashed line in Fig. 3 also shows a calculation of the pp correlation function based on the so-called Lednický model [55]. Specifically, the definition of the scattering wave function described in Eq. (89) of Ref. [55] is considered exclusively for the S-wave ($S = J = 0$) contribution. The overall antisymmetrization of the wave function and the normalization of the correlation function follow the same approach that is used for the AV18 S-wave contribution. Similar to pionless EFT at LO, the only input parameter to this calculation is

the (Coulomb-modified) S-wave scattering length a_{pp}. The predicted correlation function agrees with the pionless EFT at LO, but this model disagrees noticeably with both the AV18 calculations (with the caveat that neither the AV18 potential nor the Lednický model provides a theoretical uncertainty estimate).

B. Comparing C_{nd} using the PHH and Faddeev techniques

In this section we start our study of the Nd correlation function. We consider first the nd system in order to avoid complications due to the inclusion of the Coulomb interaction. To this end, it is convenient to write the wave function as in Eq. (24), taking into account that now the regular and irregular functions reduce to simple spherical Bessel functions, and the Coulomb phase shift σ_L is set to zero. Inserting this wave function in Eq. (14), performing the sum over m_2 and m_1 and realizing that $\int d\Omega\, \Psi^{\dagger}_{L'S'J'J'_z}\Psi_{LSJJ_z}$ clearly is not vanishing only if $J = J'$ and $J_z = J'_z$, one obtains

$$\begin{aligned} C_{nd}(k) &= \frac{1}{A_d}\frac{1}{6}4\pi \sum_{JLS}(2J+1) \\ &\quad \times \int \rho^5 d\rho d\Omega\, \frac{e^{-\rho^2/4R_M^2}}{\left(4\pi R_M^2\right)^3}\left|\Psi_{LSJJ_z}\right|^2 \\ &\equiv \sum_{JLS} C_{nd}^{LSJ}(k). \end{aligned} \tag{57}$$

Each component of the wave function Ψ_{LSJJ_z} gives a separate contribution and we can define

$$C_{nd}^{J^\pi}(k) = \sum_{LS} C_{nd}^{LSJ}(k), \tag{58}$$

where $\pi = \pm$ indicates the parity and the sum is over all the possible LS combinations for a given J and π. Then we compare the contributions from different partial waves $^{2S+1}L_J$ to the nd correlation function $C_{nd}(k)$. We use the AV18 interaction and consider the specific cases of $E = 0.3195$ MeV ($k = 20$ MeV) and $E = 2$ MeV ($k = 50$ MeV), with both the PHH method and Faddeev equations. The results are shown in Table I. As it can be seen in the table, there is an overall good agreement between the two calculations up to minor differences. The remaining small discrepancies are reflecting differences in the numerical approaches (such as configuration-space versus momentum-space discretizations and corresponding truncation schemes), and in part they are likely also due to the fact that for the Faddeev calculation isospin-breaking components within the AV18 are neglected, i.e., the np and nn interactions are taken to be exactly degenerate. We also observe that, at the energies we consider, the largest contributions are brought by the $^2S_{\frac{1}{2}}$ and ^4P_J waves.

C. Proton-deuteron correlation function

In the following we show our results for the proton-deuteron correlation function $C_{pd}(k)$, starting with the PHH calculation. As in the nd case, each component of the wave function gives a separate contribution, namely,

TABLE I. Contributions from partial waves $^{2S+1}L_J$ to the neutron-deuteron correlation function $C_{nd}(k)$ calculated at $E = 0.3195$ MeV ($k = 20$ MeV) and $E = 2$ MeV ($k = 50$ MeV) with the AV18 potential, using two different methods to perform the calculation. The source radius R_M here is chosen to be 1.5 fm.

		$k = 20$ MeV		$k = 50$ MeV	
J^π	Wave	PHH	Faddeev	PHH	Faddeev
$\frac{1}{2}^+$	$^2S_{\frac{1}{2}}$	0.42854	0.42763	0.26003	0.25950
	$^4D_{\frac{1}{2}}$	0.00004	0.00004	0.00075	0.00072
$\frac{1}{2}^-$	$^2P_{\frac{1}{2}}$	0.00262	0.00256	0.01662	0.01635
	$^4P_{\frac{1}{2}}$	0.01713	0.01655	0.07336	0.07062
$\frac{3}{2}^+$	$^4S_{\frac{3}{2}}$	0.00931	0.00883	0.01742	0.01651
	$^2D_{\frac{3}{2}}$	0.00007	0.00007	0.00234	0.00222
	$^4D_{\frac{3}{2}}$	0.00004	0.00004	0.00115	0.00110
$\frac{3}{2}^-$	$^2P_{\frac{3}{2}}$	0.00514	0.00497	0.03225	0.03146
	$^4P_{\frac{3}{2}}$	0.03588	0.03506	0.13444	0.13118
	$^4F_{\frac{3}{2}}$	0.00000	0.00000	0.00008	0.00007
$\frac{5}{2}^-$	$^4P_{\frac{5}{2}}$	0.06214	0.05900	0.25767	0.24525
	$^2F_{\frac{5}{2}}$	0.00000	0.00000	0.00007	0.00007
	$^4F_{\frac{5}{2}}$	0.00000	0.00000	0.00012	0.00010

$$\begin{aligned} C_{pd}(k) &= \frac{1}{A_d}\frac{1}{6}4\pi \sum_{JLS}(2J+1) \\ &\quad \times \int \rho^5 d\rho d\Omega\, \frac{e^{-\rho^2/4R_M^2}}{\left(4\pi R_M^2\right)^3}\left|\Psi_{LSJJ_z}\right|^2 \\ &\equiv \sum_{JLS} C_{pd}^{LSJ}(k). \end{aligned} \tag{59}$$

As before, we can define

$$C_{pd}^{J^\pi}(k) = \sum_{LS} C_{pd}^{LSJ}(k). \tag{60}$$

In Fig. 4 the pd correlation function $C_{pd}(k)$, calculated using the AV18 + UIX interaction, is shown split in the different contributions up to $J = 5/2$. For higher values of the angular momentum, the interaction gives a negligible contribution and the correlation function is therefore computed considering only the Coulomb force. In the figure this is indicated by the curve labeled "Rest," whereas the curve labeled "Total" gives the correlation function including all contributions.

Note that low values of k correspond to small values of the pd relative kinetic energy T_{pd} (as an example, $k = 10$ MeV corresponds to $T_{pd} = 79$ keV). For $k \to 0$, the effect of the Coulomb repulsion dominates and the correlation function tends rapidly to zero. In this region, the largest contribution is given by the pd waves with $L = 0$, in particular the $L = 0$, $S = J = 1/2$ wave, whereas the $L = 0$, $S = J = 3/2$ wave is suppressed at short interparticle distances due to the Pauli principle (for $S = 3/2$, all three nucleon spins may be aligned). Around $k = 60$–160 MeV, the $L = 1$, $S = 3/2$ components with total angular momentum and parity $J^\pi = 1/2^-$, $3/2^-$, and $5/2^-$ start to give sizable, resonancelike,

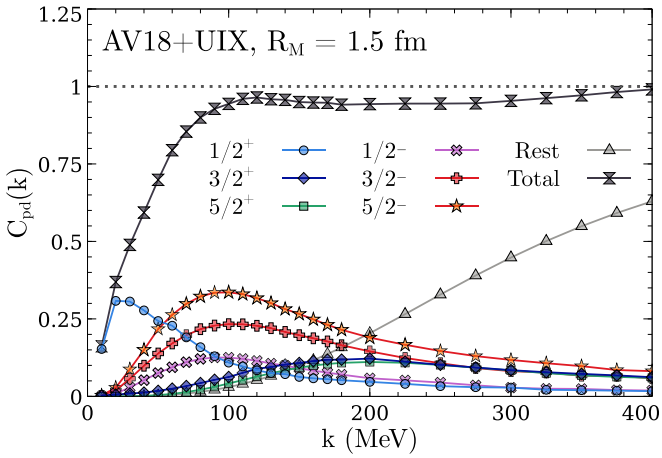

FIG. 4. The proton-deuteron correlation function $C_{pd}(k)$ and its various contributions $C_{pd}^{J^\pi}(k)$ calculated using the AV18 + UIX interaction with the PHH method. The curve labeled "Rest" shows the contribution of $J \geqslant 7/2$ states [they are taken into account via the $\Psi^{\rm free}_{m_2,m_1}$ of Eq. (31)]. The calculations are performed using a source size of $R_M = 1.5$ fm.

contributions. In fact, in those waves the effective *pd* interaction is rather attractive and the corresponding phase shifts increase very fast with energy [56]. Moreover, below $k = 200$ MeV there is a moderate splitting of the quartet $L = 1$ phases [36], and their relative contributions are nearly related by a factor $(2J + 1)$ [see Eq. (59)]. The effect from this in the total correlation function is the appearance of a wide bump with maximum located approximately at $k = 120$ MeV. At higher values of k, higher partial waves start to contribute and the correlation function tends to one.

In addition to the study of the different partial waves contribution, it is of interest to consider the correlation function calculated with different interaction models. To this aim, in Table II we show the values of the correlation function at several energies computed with the AV18 + UIX, the AV18 (without accompanying 3NF), and with the NVIa + 3N interaction. Moreover, in the fifth column (labeled by "Ratio"), the ratio between the results obtained with and without 3NF*s* is given. In this way, the effect of the three-nucleon force can be estimated, yielding that for the models considered here it is around 3% in the region close to $k = 100$ MeV.

To complete the analysis, in Fig. 5 we show the correlation function calculated with the AV18, AV18 + UIX, and NVIa + 3*N* interactions, and further compare calculations that consider only the Coulomb force and an approach based on the reduction of the wave function in the Born approximation. The latter two contributions correspond to the following approximations. The "Coulomb only" curve was obtained considering the free (i.e., pure Coulomb) *pd* relative wave function—namely, that given in Eq. (21)—with the deuteron wave function still calculated with the AV18 interaction. The difference between this curve and the one labeled "AV18" (blue diamonds) shows the importance of the inclusion of the nuclear interaction between the two clusters. The "optimized Born" curve was obtained by neglecting the first term in Eq. (26), or equivalently setting to zero all the hyperradial

TABLE II. The proton-deuteron correlation function $C_{pd}(k)$ calculated with different interaction models, using the PHH method. The source radius R_M is chosen to be 1.5 fm. The proton-deuteron relative momentum and the total kinetic energy $T_{pd} = \frac{4}{3}\frac{k^2}{M_N}$ in the c.m. are given (MeV) in the first and second column, respectively. In the fifth column we report the ratio of the AV18+UIX results (third column) and the AV18 values (fourth column).

k	T_{pd}	AV18+UIX	AV18	Ratio	NVIa+3N
10	0.08	0.1613	0.1727	0.9341	0.1610
20	0.32	0.3690	0.3928	0.9393	0.3690
30	0.72	0.4888	0.5057	0.9665	0.4886
40	1.27	0.5931	0.6027	0.9842	0.6012
50	2.00	0.6987	0.7054	0.9905	0.7072
60	2.88	0.7943	0.7802	1.0182	0.7820
70	3.91	0.8544	0.8365	1.0215	0.8536
80	5.11	0.9000	0.8792	1.0237	0.8955
90	6.47	0.9278	0.9085	1.0213	0.9210
100	7.99	0.9438	0.9272	1.0179	0.9388
110	9.66	0.9600	0.9367	1.0249	0.9546
120	11.50	0.9644	0.9406	1.0254	0.9618
130	13.50	0.9587	0.9398	1.0201	0.9559
140	15.66	0.9568	0.9375	1.0206	0.9491
150	17.97	0.9498	0.9371	1.0135	0.9431
160	20.45	0.9482	0.9336	1.0156	0.9401
170	23.08	0.9475	0.9304	1.0184	0.9369
180	25.88	0.9412	0.9274	1.0149	0.9368
200	31.95	0.9431	0.9277	1.0166	0.9370
225	40.44	0.9447	0.9308	1.0149	0.9361
250	49.92	0.9448	0.9368	1.0085	0.9432
275	60.41	0.9456	0.9427	1.0031	0.9437
300	71.89	0.9536	0.9491	1.0047	0.9483
325	84.37	0.9623	0.9545	1.0082	0.9554
350	97.85	0.9714	0.9605	1.0114	0.9631
375	112.32	0.9820	0.9668	1.0157	0.9729
400	127.80	0.9905	0.9745	1.0164	0.9862

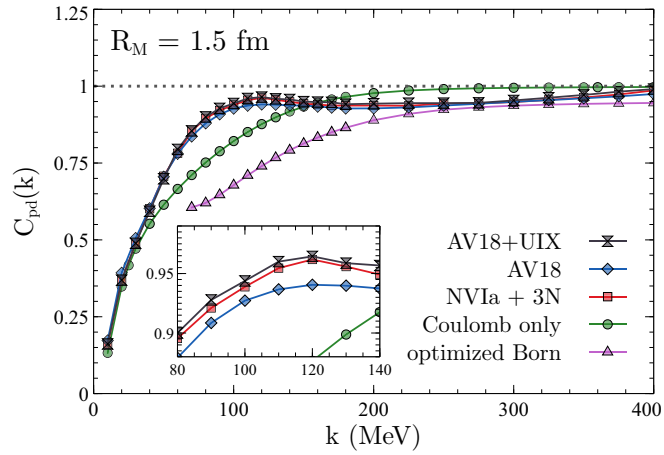

FIG. 5. The proton-deuteron correlation function $C_{pd}(k)$ calculated with different interactions and approximation of the wave function, using the PHH method. The calculations are performed using $R_M = 1.5$ fm. See the main text for more details.

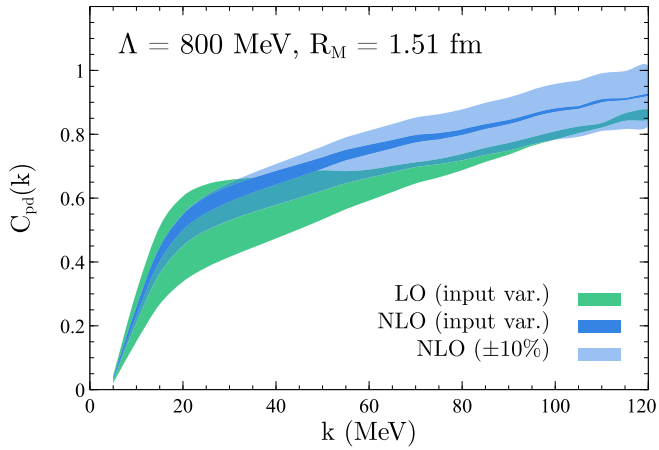

FIG. 6. Proton-deuteron correlation function calculated in pionless EFT for a source radius $R_M = 1.51$ fm. The shaded bands here represent the theoretical uncertainty from the EFT expansion. At LO, this is estimated by varying the EFT input parameters for both the ${}^3S_1$ two-body interaction as well as for the three-nucleon force (see text for details). At NLO, technical restriction at present permits us to only vary the input for the three-nucleon force, while the ${}^3S_1$ two-nucleon input remains fixed to reproduce the deuteron at its physical binding energy. As an additional lighter band we therefore include a blanket 10% variation to show a crude *a priori* estimate of the NLO uncertainty.

functions $u_{n,\alpha}(\rho)$. In this case, the wave function is approximated by the asymptotic terms given in the last four lines of Eq. (26). Then the T-matrix elements $T^J_{LS,L'S'}$ are determined from the Kohn variational principle, using that wave function as the trial input. This approximation works better for high partial waves in which the centrifugal barrier suppresses the effects of the interaction [57]. In fact, for S and P waves, this approximation gives rather different results from those obtained using the full wave function. Therefore, the difference between the curves obtained with the full wave function and that labeled "optimized Born" shows the importance of the "distortion" of the deuteron in the process. In other words, the Nd wave function at short distances is not simply given by the product of the deuteron wave function times the spin state of the third particle, but a full treatment of the three-body dynamics is necessary. Note that for $k < 60$ MeV, this "optimized Born" approximation predicts a completely wrong correlation function, which therefore has not been reported in the figure.

The main result of the pionless EFT calculation for $C_{pd}(k)$ is summarized in Fig. 6. For a fixed source radius $R_M = 1.51$ fm this figure shows the correlation function at LO and NLO in the EFT expansion as shaded bands, reflecting the theoretical uncertainty stemming from the EFT expansion. This calculation explicitly includes the nuclear interaction in pd S and P waves (which are all degenerate with respect to the total spin J at this order) and adds pure Coulomb (or Bessel, in the nd case) contributions on top of the interacting waves up to total angular momentum $\ell_{\max} = 15$.

To generate the uncertainty estimate, we have varied the input parameters that enter in the EFT renormalization conditions. Specifically, the contributions that primarily affect the calculation at LO are the ${}^3S_1$ two-nucleon interaction and the three-nucleon contact interaction. The former can be determined by reproducing either the exact deuteron binding energy or the experimental value for the scattering length in that channel. At LO, these choices are equivalent from the EFT perspective. Fitting $C_0(\Lambda)$ to reproduce the ${}^3S_1$ scattering length yields a deuteron underbound at about 1.4 MeV, which gets moved close to the experimental binding energy by perturbative NLO corrections. Similarly, the three-body interaction can be fit to reproduce either the experimental triton binding energy or the nd scattering length (either way, the splitting between the ^{3}H and ^{3}He binding energies is a prediction at this order that has been studied in great detail [46–49,53,58]). The LO band in Fig. 6 is based on the maximum variation from overall four different choices of input combinations. We chose not to vary the ${}^1S_0$ input here because the scattering length in this channel, $a_{{}^1S_0} = -23.7$ fm, is so close to the unitarity limit that small deviations from this value would hardly make any difference.

Conceptual constraints prevent us at present from performing an NLO calculation with the ${}^3S_1$ input fixed to the scattering length because, as mentioned above, range correction will shift the deuteron binding energy. Further work is required to derive a perturbative nucleon-deuteron scattering formalism that can handle the moving threshold arising from the expansion in the two-nucleon sector. The darker NLO band in Fig. 6 is therefore limited to varying the input for the three-nucleon interaction, in the same way as described above. In addition, we show a lighter NLO band generated from a ±10% variation of $C_{pd}(k)$ around the result where the three-nucleon force is fit to reproduce the nd scattering length. We note that although this approach reflects the *a priori* estimate for the pionless EFT uncertainty at NLO, it does not take into account the constraint that the correlation function should approach unity as $k \to \infty$.

Generally, that constraint would be expected to lower the NLO uncertainty. However, for larger k we observe that pd P-wave contributions start dominating over the S wave, and ultimately higher pd partial waves become sizable as well. It is known that P-wave Nd phase shifts converge relatively slowly in pionless EFT, with sizable corrections at next-to-next-to-leading order (N2LO). While that calculation is currently beyond our reach, we expect that it will improve agreement of the pionless EFT calculation with the results from potential models. Moreover, at LO and NLO, pionless EFT receives its two-nucleon input from S waves only, while all higher partial waves vanish by construction at these orders (keep in mind that the three-nucleon dynamics nevertheless induce P and higher partial waves in the Nd sector). These effects will also enter at N2LO and induce a splitting between contributions from different J for the same l_2, s_2 combination [59].

It should be noted, however, that the breakdown scale of pionless EFT is expected to be set by the pion mass $M_\pi \approx 140$ MeV. One should therefore not expect this EFT calculation to perform well for momenta k near or beyond that scale; the expansion is constructed for the low-energy regime.

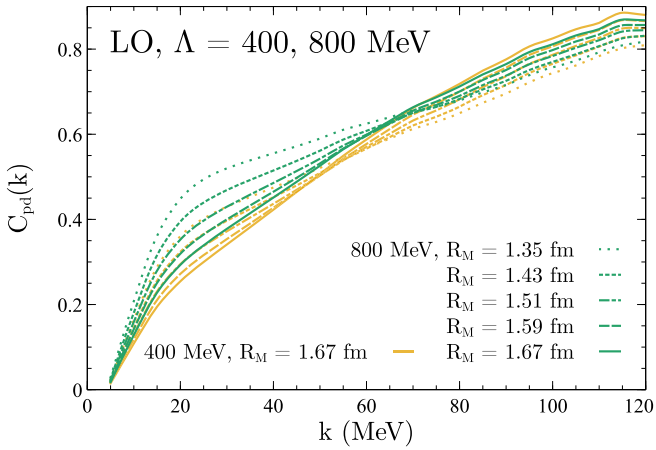

FIG. 7. The proton-deuteron correlation function $C_{pd}(k)$ calculated in pionless EFT for different EFT cutoffs Λ and source radii R_M. Orange (green) lines are used for results obtained with $\Lambda =$ 400 (800) MeV. The orange long-dashed, dot-dash, short-dashed, and dotted curves have been obtained with $\Lambda = 800$ MeV and the same R_M values as the corresponding green curves.

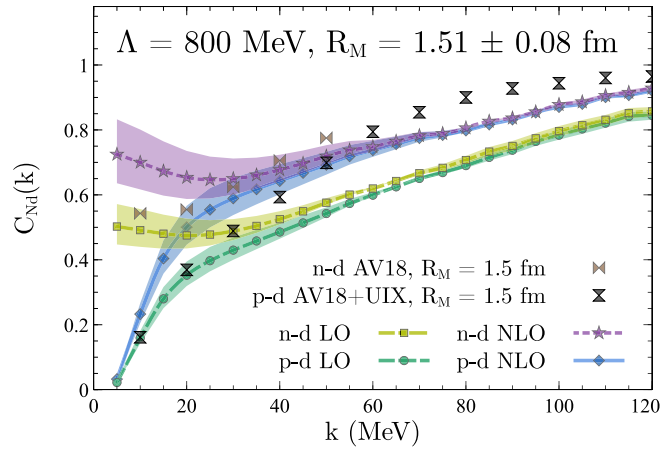

FIG. 8. The proton-deuteron and neutron-deuteron correlation functions calculated in pionless EFT with $\Lambda = 800$ MeV. The central curves show results for a source radius $R_M = 1.51$ fm, while shaded bands here indicate the result of varying the source radius by ± 0.08 fm. Double triangles show *nd* AV18 and *pd* AV18 + UIX results calculated at $R_M = 1.5$ fm for comparison.

As mentioned at the end of Sec. II C 2, for calculations above the deuteron breakup threshold we include a small imaginary part $i\eta$ in the energy to regularize an on-shell singularity. For the results shown in Fig. 6, we have used the value $\eta = 0.1$ MeV. Increasing this to $\eta = 0.5$ MeV leads to a variation of typically about 1%, which is negligible compared to other uncertainties. Similarly, we used a regulating photon mass $\lambda = 0.2$ MeV for all calculations shown here and note that variations due to alternative choices can be be safely neglected.

For the results shown in Fig. 6 we used a regulator scale (cutoff) of $\Lambda = 800$ MeV. In the diagrammatic framework we used, this is implemented with a sharp upper bound on momentum integrals at the three-nucleon level, while the two-nucleon subsector is treated using dimensional regularization. Pionless EFT, like any effective field theory, exhibits some residual cutoff dependence that should decrease in magnitude as one goes to higher orders, and it is an indication of proper renormalization that results for observables overall flatten out at large cutoffs. In Fig. 7 we show the change in the LO *pd* correlation function as one goes from $\Lambda = 400$ to $\Lambda = 800$ MeV; little additional variation is observed for larger Λ. In this figure we also use different line styles to show how the correlation function changes as we vary the source radius R_M between 1.27 and 1.59 fm.

D. Proton-deuteron versus neutron-deuteron correlation function

In Fig. 8 we compare the correlation functions for *pd* and *nd* systems. For this comparison we keep the EFT input parameters fixed (with the $^3S_1$ channel fixed to reproduce the deuteron binding energy and the three-nucleon force fit to the *nd* scattering length) and show as shaded bands the result of varying the source radius R_M around a central value of 1.51 fm. Consistent with the expectation that Coulomb effects should be a perturbative effect anywhere except at the lowest energies, we observe that the *pd* and *nd* curves in Fig. 8 approach one another with increasing momentum k.

We include in Fig. 8 also results obtained for the *nd* correlation function with the AV18 potential (without additional three-nucleon force, calculated in momentum space via Faddeev equations), as well as for the *pd* correlation function from an AV18 + UIX potential (calculated in coordinate space via the PHH method). For these calculations we use a source radius $R_M = 1.5$ fm. Overall these results and the pionless EFT calculation are in reasonable agreement, in particular if one keeps in mind that in this figure we do not indicate EFT uncertainty bands on top of the source-radius variation. Some mild tension between the EFT NLO results and potential models *might* exist in the low-k region. Noting that even at small k there is a sizable shift from LO to NLO in the EFT results, we believe that an N2LO calculation, which would include NN P-wave interactions as well as effects from the $^3S_1 - {}^3D_1$ mixing induced by the nuclear tensor force, is likely to narrow the discrepancy between the different interactions.

IV. SUMMARY AND OUTLOOK

Femtoscopic analyses of correlation functions extracted from high-energy collisions of protons and nuclei have opened the door to new studies of low-energy scattering processes in light systems such as pd, Λd, ppp, $pp\Lambda$, and many others. Measurements of correlations in these systems have recently been performed, or are planned by the ALICE Collaboration in the near future. Accordingly, methods that have been applied in recent years to calculate scattering observables can be used to obtain the above-mentioned correlation functions. The present study that performs a detailed analysis of the Nd correlation functions is the first step in this direction. Although the *nd* correlation function, $C_{nd}(k)$, cannot be measured at present since neutron detectors are not being used in the relevant experiments, its study serves to compare different

methods, such as the Faddeev and PHH techniques. In fact, the *nd* system does not present the challenge of treating the long-range Coulomb interaction. In this work, the AV18 potential has been used to make comparisons for $C_{nd}(k)$, with the conclusion that the PHH technique and the solution of the Faddeev equations produce extremely close results. This study, which directly involves the scattering wave functions, extends to some extent previous benchmarks done between these techniques [41].

The next step in this work has been to use the PHH wave functions obtained for AV18 and other nuclear potential models to compute the *pd* correlation function $C_{pd}(k)$ in a broad energy range, in order to enable detailed comparisons to current and upcoming measurements. The ALICE Collaboration has presented preliminary results for the *pd* correlation function measured in proton-proton collisions [60] and final results are expected to be published soon. The correlation function, as a function of the energy, has some structure produced by the interplay of contributions from different partial waves. At low energies the system in relative S wave is dominant, whereas a peak around values of $k = 120$ MeV appears when the relative P wave starts to dominate. These are the partial waves in which the short-range nuclear interaction produces the largest effect. Due to the centrifugal barrier, higher partial waves are mostly dominated by the Coulomb interaction. All these considerations have been presented in dedicated figures and tables. In particular, we have considered the impact of different interactions, with and without the inclusion of three-nucleon forces, on the correlation functions. The conclusion is that within the context of potential models different interactions give very small variations, not above 1% effects, whereas the three-nucleon force produces changes of around 2% in the observable. Since the correlation function is an integral observable, effects of this kind are expected to be small. However, a 2% effect is likely within the reach of the next experimental runs planned by the ALICE Collaboration, and this is one of the main indications of the present analysis. In addition to phenomenological potential models, we have also performed a pionless EFT calculation of the correlation function, going up to next-to-leading order in the EFT expansion in a rigorously perturbative setup. Within the theoretical uncertainty of the EFT, we find overall good agreement with the potential-model calculations in the low-energy regime where the EFT is applicable.

To compute the correlation function, two ingredients are needed: the source function and the scattering wave function. The size of the source is determined by the size of the emitting nucleon source and it is fixed by the analysis of the transverse mass m_T [defined as $m_T = (k_T^2 + m^2)^{1/2}$, where m is the average mass and k_T is the transverse momentum of the pair]. A precise determination of the dependence of the source size with the transverse mass m_T has been realized in proton-proton collisions [22]. For the present analysis, the source term is characterized by the effective nucleon-nucleon distance and depends on the m_T of the emitted *pd* pairs. The value of $R_M = 1.5$ fm was used in this paper because it is close to the value that gives the best description of the preliminary $C_{pd}(k)$ data from the ALICE Collaboration [60].

Overall, we can draw two main conclusions: The first is that the nucleon-deuteron scattering wave function, calculated in the present analysis with a full account of the three-body dynamics, introduces a complex dynamical behavior in the correlation function through the relative importance of different partial waves, in particular the interplay between S and P waves. Second, we show that over the considered range of momenta up to 400 MeV, the correlation function is sensitive to aspects of the nuclear interaction, in the present work constructed as a sum of two- and three-nucleon contributions. We conclude that the present study supports the experimental efforts devoted to measuring the correlation function in light nuclear systems dominated by the strong interaction. This conclusion is particularly promising in the study of the systems with strangeness, where information on the dynamics (as, for example, the $pp\Lambda$ three-body force) is hardly obtained in other experimental investigations.

ACKNOWLEDGMENTS

We thank Laura Fabbietti, Johann Haidenbauer, and Stanislaw Mrówczyński for useful discussions. S.K. acknowledges discussions with participants of the INT Program INT-23-1a, "Intersection of nuclear structure and high-energy nuclear collisions," thanks the Institute for Nuclear Theory for its hospitality. This work was supported in part by the National Science Foundation under Grant No. PHY–2044632. This material is based upon work supported by the U.S. Department of Energy, Office of Science, Office of Nuclear Physics, under the FRIB Theory Alliance, Award No. DE-SC0013617. Computational resources for parts of this work were provided by the Jülich Supercomputing Center as well as by the high-performance computing cluster operated by North Carolina State University. We also gratefully acknowledge the support of the INFN-Pisa computing center.

[1] I. Bombaci and D. Logoteta, Equation of state of dense nuclear matter and neutron star structure from nuclear chiral interactions, Astron. Astrophys. **609**, A128 (2018).

[2] C. Drischler, J. Holt, and C. Wellenhofer, Chiral effective field theory and the high-density nuclear equation of state, Annu. Rev. Nucl. Part. Sci. **71**, 403 (2021).

[3] J. Lattimer, Neutron stars and the nuclear matter equation of state, Annu. Rev. Nucl. Part. Sci. **71**, 433 (2021).

[4] A. Deltuva, A. Fonseca, and P. Sauer, Nuclear many-body scattering calculations with the Coulomb interaction, Annu. Rev. Nucl. Part. Sci. **58**, 27 (2008).

[5] W. Leidemann and G. Orlandini, Modern ab initio approaches and applications in few-nucleon physics with $a \geqslant 4$, Prog. Part. Nucl. Phys. **68**, 158 (2013).

[6] P. Navrátil, S. Quaglioni, G. Hupin, C. Romero-Redondo, and A. Calci, Unified ab initio approaches to

nuclear structure and reactions, Phys. Scr. **91**, 053002 (2016).
[7] P. Navratil and S. Quaglioni, Ab initio nuclear reaction theory with applications to astrophysics, arXiv:2204.01187.
[8] W. Glöckle, H. Witała, D. Hüber, H. Kamada, and J. Golak, The three-nucleon continuum: Achievements, challenges and applications, Phys. Rep. **274**, 107 (1996).
[9] J. Golak, R. Skibinski, H. Witala, W. Glockle, A. Nogga, and H. Kamada, Electron and photon scattering on three-nucleon bound states, Phys. Rep. **415**, 89 (2005).
[10] M. H. Wood, C. R. Brune, B. M. Fisher, H. J. Karwowski, D. S. Leonard, E. J. Ludwig, A. Kievsky, S. Rosati, and M. Viviani, Low-energy *p-d* scattering: High-precision data, comparisons with theory, and phase-shift analyses, Phys. Rev. C **65**, 034002 (2002).
[11] A. Deltuva, A. C. Fonseca, and P. U. Sauer, Momentum-space description of three-nucleon breakup reactions including the Coulomb interaction, Phys. Rev. C **72**, 054004 (2005); [Erratum: **72**, 059903(E) (2005)].
[12] R. B. Wiringa, V. G. J. Stoks, and R. Schiavilla, An accurate nucleon-nucleon potential with charge independence breaking, Phys. Rev. C **51**, 38 (1995).
[13] V. G. J. Stoks, R. A. M. Klomp, C. P. F. Terheggen, and J. J. de Swart, Construction of high-quality *NN* potential models, Phys. Rev. C **49**, 2950 (1994).
[14] R. Machleidt, High-precision, charge-dependent Bonn nucleon-nucleon potential, Phys. Rev. C **63**, 024001 (2001).
[15] P. Reinert, H. Krebs, and E. Epelbaum, Semilocal momentum-space regularized chiral two-nucleon potentials up to fifth order, Eur. Phys. J. A **54**, 86 (2018).
[16] S. K. Saha, D. R. Entem, R. Machleidt, and Y. Nosyk, Local position-space two-nucleon potentials from leading to fourth order of chiral effective field theory, Phys. Rev. C **107**, 034002 (2023).
[17] A. Nogga, R. G. E. Timmermans, and U. van Kolck, Renormalization of one-pion exchange and power counting, Phys. Rev. C **72**, 054006 (2005).
[18] H.-W. Hammer, S. König, and U. van Kolck, Nuclear effective field theory: Status and perspectives, Rev. Mod. Phys. **92**, 025004 (2020).
[19] L. Girlanda, E. Filandri, A. Kievsky, L. E. Marcucci, and M. Viviani, Effect of the N3LO three-nucleon contact interaction on *p-d* scattering observables, Phys. Rev. C **107**, L061001 (2023).
[20] S. Acharya *et al.* (ALICE Collaboration), $p-p$, $p-\Lambda$ and $\Lambda-\Lambda$ correlations studied via femtoscopy in *pp* reactions at $\sqrt{s}=7$ TeV, Phys. Rev. C **99**, 024001 (2019).
[21] S. Acharya *et al.* (ALICE Collaboration), Investigation of the p–Σ_0 interaction via femtoscopy in pp collisions, Phys. Lett. B **805**, 135419 (2020).
[22] S. Acharya *et al.* (ALICE Collaboration), Search for a common baryon source in high-multiplicity pp collisions at the LHC, Phys. Lett. B **811**, 135849 (2020).
[23] C. B. Chitwood *et al.*, Final-state interactions between noncompound light particles for ^{16}O-induced reactions on ^{197}Au at $E/A=25$ MeV, Phys. Rev. Lett. **54**, 302 (1985).
[24] J. Pochodzalla *et al.*, External Coulomb distortion of proton-deuteron final-state interactions for induced reactions on Au at $E/A=35$ MeV, Phys. Lett. B **175**, 275 (1986).
[25] J. Pochodzalla *et al.*, Two-particle correlations at small relative momenta for ^{40}induced reactions on ^{197}Au at $E/A=60$ MeV, Phys. Rev. C **35**, 1695 (1987).
[26] K. Wosińska *et al.*, Correlations of neutral and charged particles in ^{40}Ar - ^{58}Ni reaction at 77 MeV/u, Eur. Phys. J. A. **32**, 55 (2007).
[27] B. S. Pudliner, V. R. Pandharipande, J. Carlson, and R. B. Wiringa, Quantum Monte Carlo calculations of $A\leqslant 6$ nuclei, Phys. Rev. Lett. **74**, 4396 (1995).
[28] M. Piarulli, L. Girlanda, R. Schiavilla, R. N. Pérez, J. E. Amaro, and E. R. Arriola, Minimally nonlocal nucleon-nucleon potentials with chiral two-pion exchange including Δ resonances, Phys. Rev. C **91**, 024003 (2015).
[29] A. Baroni *et al.*, Local chiral interactions, the tritium Gamow-Teller matrix element, and the three-nucleon contact term, Phys. Rev. C **98**, 044003 (2018).
[30] U. W. Heinz and B. V. Jacak, Two particle correlations in relativistic heavy ion collisions, Annu. Rev. Nucl. Part. Sci. **49**, 529 (1999).
[31] S. Mrówczyński, Production of light nuclei at colliders—coalescence vs. thermal model, Eur. Phys. J. Spec. Top. **229**, 3559 (2020).
[32] M. A. Lisa, S. Pratt, R. Soltz, and U. Wiedemann, Femtoscopy in relativistic heavy ion collisions, Annu. Rev. Nucl. Part. Sci. **55**, 357 (2005).
[33] S. E. Koonin, Proton pictures of high-energy nuclear collisions, Phys. Lett. B **70**, 43 (1977).
[34] L. E. Marcucci, J. Dohet-Eraly, L. Girlanda, A. Gnech, A. Kievsky, and M. Viviani, The hyperspherical harmonics method: A tool for testing and improving nuclear interaction models, Front. Phys. **8**, 69 (2020).
[35] A. Kievsky, S. Rosati, M. Viviani, L. E. Marcucci, and L. Girlanda, A high-precision variational approach to three- and four-nucleon bound and zero-energy scattering states, J. Phys. G: Nucl. Part. Phys. **35**, 063101 (2008).
[36] A. Kievsky, M. Viviani, and S. Rosati, Polarization observables in $p-d$ scattering below 30 MeV, Phys. Rev. C **64**, 024002 (2001).
[37] A. Kievsky, M. Viviani, and L. E. Marcucci, *n-d* scattering including electromagnetic forces, Phys. Rev. C **69**, 014002 (2004).
[38] H. A. Bethe, Theory of the effective range in nuclear scattering, Phys. Rev. **76**, 38 (1949).
[39] P. F. Bedaque, H.-W. Hammer, and U. van Kolck, Renormalization of the three-body system with short-range interactions, Phys. Rev. Lett. **82**, 463 (1999).
[40] P. F. Bedaque, H.-W. Hammer, and U. van Kolck, Effective theory of the triton, Nucl. Phys. A **676**, 357 (2000).
[41] D. Hüber, W. Glöckle, J. Golak, H. Witała, H. Kamada, A. Kievsky, S. Rosati, and M. Viviani, Realistic phase shift and mixing parameters for elastic neutron-deuteron scattering: Comparison of momentum space and configuration space methods, Phys. Rev. C **51**, 1100 (1995).
[42] C. R. Chen, G. L. Payne, J. L. Friar, and B. F. Gibson, Low-energy nucleon-deuteron scattering, Phys. Rev. C **39**, 1261 (1989).
[43] F. Tabakin and K. T. R. Davies, Smooth velocity-dependent potential and nuclear matter, Phys. Rev. **150**, 793 (1966).
[44] X. Kong and F. Ravndal, Coulomb effects in low energy proton-proton scattering, Nucl. Phys. A **665**, 137 (2000).

[45] G. Rupak and X.-W. Kong, Quartet S-wave $p-d$ scattering in EFT, Nucl. Phys. A **717**, 73 (2003).
[46] S. König and H.-W. Hammer, Low-energy $p-d$ scattering and ^{3}He in pionless EFT, Phys. Rev. C **83**, 064001 (2011).
[47] J. Vanasse, D. A. Egolf, J. Kerin, S. König, and R. P. Springer, ^{3}He and pd scattering to next-to-leading order in pionless effective field theory, Phys. Rev. C **89**, 064003 (2014).
[48] S. König, H. W. Grießhammer, H.-W. Hammer, and U. van Kolck, Effective theory of ^{3}H and ^{3}He, J. Phys. G: Nucl. Part. Phys. **43**, 055106 (2016).
[49] J. Kirscher and D. Gazit, The Coulomb interaction in helium-3: Interplay of strong short-range and weak long-range potentials, Phys. Lett. B **755**, 253 (2016).
[50] S. König, Second-order perturbation theory for ^{3}He and pd scattering in pionless EFT, J. Phys. G: Nucl. Part. Phys. **44**, 064007 (2017).
[51] S. König, H. W. Grießhammer, H.-W. Hammer, and U. van Kolck, Nuclear physics around the unitarity limit, Phys. Rev. Lett. **118**, 202501 (2017).
[52] P. F. Bedaque, H.-W. Hammer, and U. van Kolck, The three-boson system with short-range interactions, Nucl. Phys. A **646**, 444 (1999).
[53] S. König, H. W. Grießhammer, and H. W. Hammer, The proton-deuteron system in pionless EFT revisited, J. Phys. G: Nucl. Part. Phys. **42**, 045101 (2015).
[54] S. König, Energies and radii of light nuclei around unitarity, Eur. Phys. J. A **56**, 113 (2020).
[55] R. Lednicky, Finite-size effects on two-particle production in continuous and discrete spectrum, Phys. Part. Nuclei **40**, 307 (2009).
[56] A. Kievsky, J. L. Friar, G. L. Payne, S. Rosati, and M. Viviani, Phase shifts and mixing parameters for low-energy proton-deuteron scattering, Phys. Rev. C **63**, 064004 (2001).
[57] A. Kievsky, S. Rosati, W. Tornow, and M. Viviani, Critical comparison of experimental data and theoretical predictions for N-d scattering below the breakup threshold, Nucl. Phys. A **607**, 402 (1996).
[58] S.-i. Ando and M. C. Birse, Effective field theory of ^{3}He, J. Phys. G: Nucl. Part. Phys. **37**, 105108 (2010).
[59] J. Vanasse, Fully perturbative calculation of nd scattering to next-to-next-to-leading order, Phys. Rev. C **88**, 044001 (2013).
[60] B. Singh, Extending the ALICE strong-interaction studies to nuclei: Measurement of proton-deuteron correlations in pp collisions at $\sqrt{s} = 13$ TeV, Proc. Sci. **EPS-HEP2021**, 391 (2022).